Human umbilical cord mesenchymal stem cell-derived exosomes ameliorate liver steatosis by promoting fatty acid oxidation and reducing fatty acid synthesis
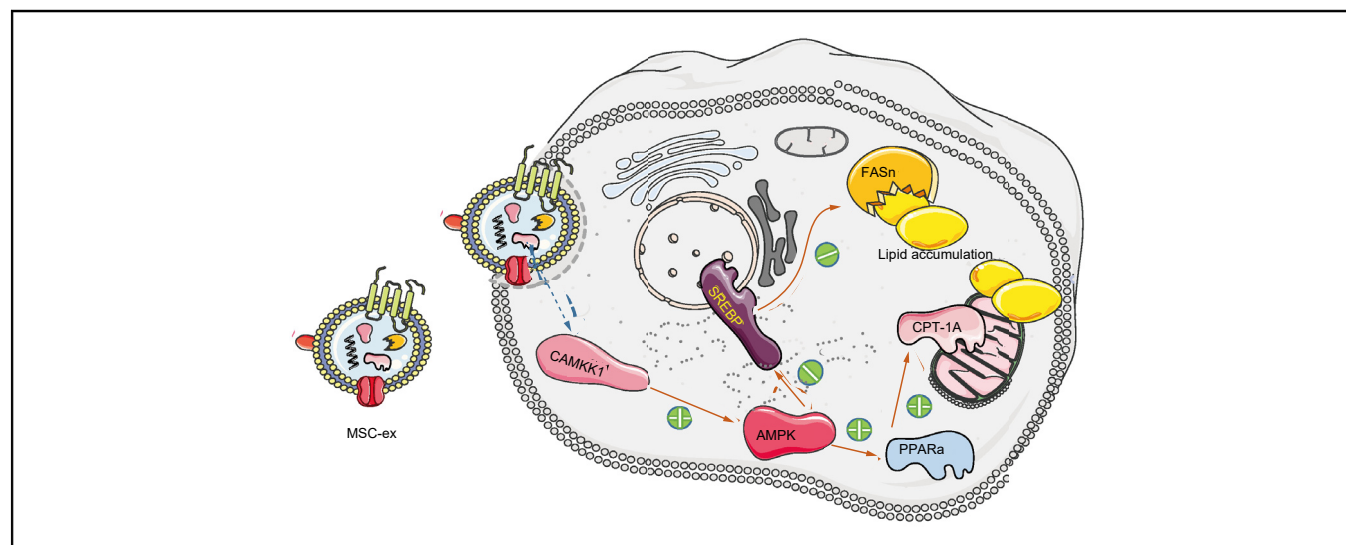
Authors
Fuji Yang, **Yanshuang Wu**, **Yifei Chen**, Jianbo Xi, Ying Chu, Jianhua Jin, Yongmin Yan

Correspondence
yym@wjrmyy.cn (Y. Yan), jinjianhua@wjrmyy.cn (J. Jin).

Graphical abstract

Highlights

- MSC-derived exosomes ameliorate liver steatosis in NAFLD mice.

- MSC-ex-transferred CAMKK1 is responsible for reducing lipid accumulation.

- CAMKK1 inhibits SREBP-1C-mediated fatty acid synthesis and enhances PPARα-mediated fatty acid oxidation in an AMPK-dependent manner.

Impact and Implications

NAFLD includes many conditions, from simple steatosis to non-alcoholic steatohepatitis, which can lead to fibrosis, cirrhosis, and even hepatocellular carcinoma. So far, there is no approved drug for treating liver steatosis of NAFLD. Thus, better therapies are needed to regulate lipid metabolism and prevent the progression from liver steatosis to chronic liver disease. By using a combination of non-targeted lipidomic and transcriptome analyses, we revealed that human umbilical cord mesenchymal stem cell-derived exosomes (MSC-ex) effectively reduced lipid deposition and improved liver function from HFD-induced liver steatosis. Our study highlights the importance of exosomal CAMKK1 from MSC-ex in mediating lipid metabolism regulation via AMPK-mediated PPARα/CPT-1A and SREBP-1C/fatty acid synthase signalling in hepatocytes. These findings are significant in elucidating novel mechanisms related to MSC-ex-based therapies for preventing NAFLD.

Human umbilical cord mesenchymal stem cell-derived exosomes ameliorate liver steatosis by promoting fatty acid oxidation and reducing fatty acid synthesis

Fuji Yang,[1,2,†] **Yanshuang Wu**,[2,3,†] **Yifei Chen**,[2,†] Jianbo Xi,[4] Ying Chu,[1,4] Jianhua Jin,[4,*] Yongmin Yan[1,4,*]

[1]*Department of Laboratory Medicine, Wujin Hospital Affiliated with Jiangsu University, Jiangsu University, Changzhou, China;* [2]*School of Medicine, Jiangsu University, Zhenjiang, China;* [3]*Department of Laboratory Medicine, The Affiliated Hospital of Xuzhou Medical University, Xuzhou, China;* [4]*Changzhou Key Laboratory of Molecular Diagnostics and Precision Cancer Medicine, Wujin Hospital Affiliated with Jiangsu University (Wujin Clinical College of Xuzhou Medical University), Changzhou, China*

Background & Aims: Non-alcoholic fatty liver disease (NAFLD) affects nearly a quarter of the population with no approved pharmacological therapy. Liver steatosis is a primary characteristic of NAFLD. Recent studies suggest that human umbilical cord mesenchymal stem cell-derived exosomes (MSC-ex) may provide a promising strategy for treating liver injury; however, the role and underlying mechanisms of MSC-ex in steatosis are not fully understood.
Methods: Oleic–palmitic acid-treated hepatic cells and high-fat diet (HFD)-induced NAFLD mice were established to observe the effect of MSC-ex. Using non-targeted lipidomics and transcriptome analyses, we analysed the gene pathways positively correlated with MSC-ex. Mass spectrometry and gene knockdown/overexpression analyses were performed to evaluate the effect of calcium/calmodulin-dependent protein kinase 1 (CAMKK1) transferred by MSC-ex on lipid homoeostasis regulation.
Results: Here, we demonstrate that MSC-ex promote fatty acid oxidation and reduce lipogenesis in oleic–palmitic acid-treated hepatic cells and HFD-induced NAFLD mice. Non-targeted lipidomics and transcriptome analyses suggested that the effect of MSC-ex on lipid accumulation positively correlated with the phosphorylation of AMP-activated protein kinase. Furthermore, mass spectrometry and gene knockdown/overexpression analyses revealed that MSC-ex-transferred CAMKK1 is responsible for ameliorating lipid accumulation in an AMP-activated protein kinase-dependent manner, which subsequently inhibits SREBP-1C-mediated fatty acid synthesis and enhances peroxisome proliferator-activated receptor alpha (PPARα)-mediated fatty acid oxidation.
Conclusions: MSC-ex may prevent HFD-induced NAFLD via CAMKK1-mediated lipid homoeostasis regulation.
Impact and Implications: NAFLD includes many conditions, from simple steatosis to non-alcoholic steatohepatitis, which can lead to fibrosis, cirrhosis, and even hepatocellular carcinoma. So far, there is no approved drug for treating liver steatosis of NAFLD. Thus, better therapies are needed to regulate lipid metabolism and prevent the progression from liver steatosis to chronic liver disease. By using a combination of non-targeted lipidomic and transcriptome analyses, we revealed that human umbilical cord mesenchymal stem cell-derived exosomes (MSC-ex) effectively reduced lipid deposition and improved liver function from HFD-induced liver steatosis. Our study highlights the importance of exosomal CAMKK1 from MSC-ex in mediating lipid metabolism regulation via AMPK-mediated PPARα/CPT-1A and SREBP-1C/fatty acid synthase signalling in hepatocytes. These findings are significant in elucidating novel mechanisms related to MSC-ex-based therapies for preventing NAFLD.

Introduction

Non-alcoholic fatty liver disease (NAFLD) affects nearly 24% of the world's population and is considered a major global public health concern of the 21st century.[1,2] Reduced hepatic fatty acid oxidation and increased fatty acid synthesis are key lipotoxic triggers driving hepatocyte injury, inflammation, and liver steatosis. Currently, no approved pharmacological interventions are available to prevent or ameliorate liver steatosis.[3] Thus, better therapies are needed to regulate lipid metabolism and prevent the progression of liver steatosis to chronic liver disease.

Mesenchymal stem cells (MSCs) have recently been considered as a modality for cell therapy for liver dysfunction. Several preclinical and clinical studies have shown that MSCs from bone marrow, umbilical cord, and adipose exhibit therapeutic potential in acute and chronic liver failure.[4–6] However, viable MSC-based therapies may also be accompanied by risks of undesired

differentiation, poor engraftment, immune rejection, or malignant transformation.[7,8] The therapeutic potential of MSC transplantation has been mainly attributed to paracrine activity.[9] Exosomes are natural nanosized vesicles (30∼150 nm) secreted by various cells and are also promising drug delivery carriers. For therapeutic purposes, exosomes can be produced in large quantities using cells with high proliferative capabilities, for example, MSCs.[9,10] These exosomes present a natural drug delivery vehicle as they do not have adverse effects and may be able to target specific tissues. Exosomes are also ideal modes of drug delivery as they have an extended circulating half-life and biocompatibility. Furthermore, exosomes can surpass the blood–brain barrier. Several studies have shown that human umbilical cord MSC-derived exosomes (MSC-ex) can regenerate and repair damaged liver tissues in CCl_4-induced hepatic injury and fibrosis.[11–13] Cheng *et al.*[14] confirmed that MSC-ex can down-regulate lipid metabolism-related gene expression and reduce lipid deposition in NAFLD rats. Watanabe *et al.*[15] found that adipose MSC-derived small extracellular vesicles alleviate liver fibrosis in a rapid non-alcoholic steatohepatitis fibrosis model. Furthermore, MSC-ex improve hepatic glucose and lipid metabolism in type 2 diabetes mellitus rats by activating autophagy.[16] However, the effects of MSC-ex on lipid metabolism regulation against steatosis are not fully understood, and the underlying mechanisms remain unknown.

In the current study, a high-fat diet (HFD)-induced liver steatosis model was used to examine the beneficial potential of MSC-ex on liver steatosis. MSC-ex were shown to prevent hepatic deposition and improve liver function. Moreover, MSC-ex inhibited lipid accumulation in hepatocytes by enhancing the β-oxidation of fatty acids and reducing the generation of fatty acid metabolites. By using a combination of non-targeted lipidomics and transcriptome analyses, we revealed that the AMP-activated protein kinase (AMPK) signalling pathway plays a vital role in MSC-ex-mediated lipid metabolism regulation. We further demonstrated that calcium/calmodulin-dependent protein kinase 1 (CAMKK1) is an essential factor in MSC-ex-mediated anti-hepatic steatosis and that it reduces lipid accumulation in an AMPK-dependent manner by inhibiting sterol regulatory element-binding protein-1C (SREBP-1C)-mediated fatty acid synthesis and enhancing peroxisome proliferator-activated receptor alpha (PPARα)-mediated fatty acid oxidation.

Materials and methods

Cell culture

MSCs were isolated and maintained in serum-free DMEM (Life Technologies, Carlsbad, CA, USA).[17] Human hepatocyte cell line L02, human lung fibroblast 1 (HFL1), alpha mouse liver 12 (AML12), and human embryonic kidney (HEK293T) cells used in this study were purchased from the Chinese Academy of Sciences (Shanghai, China). L02 cells were cultured in RPMI-1640 medium (Gibco, CA, USA) comprising 10% FBS (Invitrogen, CA, USA) and 100 U penicillin/streptomycin (Invitrogen, USA). HFL1 and AML12 were maintained in a serum-free DMEM comprising 10% FBS, and 293T cells were cultured in DMEM/F12 high glucose comprising 10% FBS. To induce steatosis, L02 and 293T cells were exposed to a 2 mmol/L oleic–palmitic acid (OPA) mixture for 24 h.[18] The OPA mixture included oleic acid (C18:1) and palmitic acid (C16:0) (Sigma, St. Louis, MO, USA) at a 2:1 ratio dissolved in 5% bovine serum albumin solution (dilution in PBS).

Isolation and characterisation of MSC-ex

MSCs were isolated and characterised as previously described.[17] The cells in passages 3–4 were used for collecting exosomes. MSC-ex and foetal HFL1-derived exosomes (HFL1-ex) from cell culture supernatant were obtained by ultracentrifugation.[19,20] Briefly, MSCs and HFL1 were cultured in serum-free DMEM (ExCell Bio, Shanghai, China) for 48 h. When the cells reached 50% confluence, the conditioned medium was collected and centrifuged at 300 × g for 10 min, 2,000 × g and 10,000 × g for 30 min respecively to remove cells and cell debris. The clarified supernatant was then concentrated with a 100-kDa molecular weight cut-off (MWCO) hollow fibre membrane (Millipore, Billerica, MA, USA) at 1,000 × g for 30 min. The concentrated supernatant was ultracentrifuged at 100,000 × g for 70 min (Optima L-90K; Beckman Coulter, Brea, CA, USA). The exosome-enriched fraction was collected from the bottom of the tube and washed three times with PBS by centrifugation at 1,500 × g for 30 min with 100-kDa MWCO. Final exosomes were passed through a 0.22-mm filter and stored at −80 °C. A BCA Protein Assay Kit (CWBIO, Beijing, China) was used to determine the protein concentration of exosomes to represent the number of exosomes. The morphologies of the exosomes were visualised by transmission electron microscopy (TEM; FEI Tecnai 12, Philips, Eindhoven, The Netherlands) and atomic force microscopy (AFM; MultiMode 8, Bruker, MD, USA). Concentrations and size distribution of MSC-ex and HFL1-ex were detected using a Nanosight LM10 system (Nanosight, Amesbury, UK) and particle-tracking and fast video capture software. Expression of exosome markers Alix, TSG101, CD63, and CD9, and endoplasmic reticulum protein calnexin was analysed by immunoblotting.

Liquid chromatography–tandem MS analysis of MSC-ex

A 4 μg sample of MSC-ex and HFL1-ex peptides was taken from the autosampler using an LC-20AD nano HPLC pump (Shimadzu, Kyoto, Japan) into a C18 capture column at a rate of 8 μl/min and then eluted to a C18 analytical column (inner diameter 75 μm). The sample was passed through at a flow rate of 300 nl/min and eluted with 35% B solution (95% acetonitrile, 0.1% trifluoroacetic acid) for 40 min, followed by a linear gradient to 80% for 5 min and 80% B solution for 4 min. The eluted peptides were nano-electrospray ionised into a tandem mass spectrometer Q Exactive (Thermo Fisher Scientific, San Jose, CA, USA). Orbitrap detects complete peptides with a resolution of 70,000, the collision mode is high-energy collision dissociation, and Orbitrap detects ion fragments with a resolution of 17,500. The data rely on mass spectrometry (MS) scans with a dynamic time of 10 s alternating in cycles of 1 MS and 15 tandem MS (MS/MS) of the most abundant precursor ions. The electrospray voltage was 1.6 kV, and the first-order scanning range of MS was 350–1,800 m/z.

Proteins identified by MS were annotated and analysed for functional enrichment using PANTHER software (Protein Analysis Through Evolutionary Relationships; http://www.pantherdb.org).

Immunoblotting

Protein samples were isolated from cultured cells and animals, and the concentrations were measured using a BCA Protein Assay Kit (CWBIO) and used for subsequent immunoblotting experiments. A 10% SDS-PAGE gel was used to separate equal amounts of protein in each group and then transferred to polyvinylidene fluoride membranes. The membranes were incubated with the primary antibody at 4 °C overnight and then with the

secondary antibody at room temperature for 1 h. The protein levels were normalised to the levels of β-actin and quantified using ImageJ 7.0 software (National Institutes of Health, Bethesda, USA). The primary antibodies were as follows: CAMKK1 (ABclonal, Wuhan, China; Rabbit, polyclonal, 1:1,000), CAMKK1 (Santa Cruz Biotechnology, Dallas, TX, USA; mouse, monoclonal, 1:500), phosphorylated AMPK (p-AMPK) (Bioworld, MN, USA; rabbit, polyclonal, 1:500), AMPK (Bioworld; rabbit, polyclonal, 1:500), PPARα (Proteintech, Chicago, IL, USA; rabbit, polyclonal, 1:500), carnitine palmitoyltransferase 1A (CPT-1A) (Proteintech; rabbit, polyclonal, 1:500), SREBP-1C (Proteintech; rabbit, polyclonal, 1:2,000), fatty acid synthase (FASn) (Santa Cruz; mouse, monoclonal, 1:500), protein kinase AMP-activated non-catalytic subunit gamma 1 (PRKAG1) (Proteintech; Rabbit, polyclonal, 1:2,000), insulin growth factor-like family member 2 (IGFL2) (Bioworld; rabbit, polyclonal, 1:500), phosphorylated insulin receptor substrate 1 (p-IRS1) (Invitrogen; rabbit, polyclonal, 1:500), insulin receptor substrate 1 (IRS1) (Proteintech; rabbit, polyclonal, 1:500), CD9 (Abcam, Cambridge Science Park, UK; rabbit, monoclonal, 1:500), CD63 (Abcam; mouse, monoclonal, 1:500), CD81 (Abcam; mouse, monoclonal, 1:500), calnexin (Abcam; rabbit, monoclonal, 1:2,000), tumour susceptibility gene 101 (TSG101) (Abcam; rabbit, monoclonal, 1:500), Alix (Abcam; mouse, monoclonal, 1:500), and β-actin (ABclonal; rabbit, polyclonal, 1:2,000). The secondary antibodies were horseradish peroxidase-conjugated goat anti-rabbit and goat anti-mouse (CWBIO; 1:2,000).

HFD-induced mouse model and MSC-ex injection

C57BL/6 mice (male, 19 ± 1 g) were used to establish the NAFLD model as described.[21] All animals sustained a 12-h/12-h light/dark cycle at 23 ± 2 °C and a relative environmental humidity of 55 ± 5%. After acclimatisation for 1 week, the experimental mice were randomly assigned into five groups, namely normal chow diet-fed (10% kcal from fat) mice (normal group), HFD-fed (45% kcal from fat) mice control (HFD group), HFD-fed mice treated with MSC-ex (10 mg/kg), HFD-fed mice treated with HFL1-ex (10 mg/kg), and HFD-fed mice treated with MSC-ex-free conditional medium supernatant (deMSC-ex). For shCAMKK1 knockdown experiments, groups of HFD-fed mice were treated with MSC-ex[shCtr] or MSC-ex[shCAMKK1] (10 mg/kg) for 4 weeks. After 10 weeks, MSC-ex, MSC-ex[shCtr], and MSC-ex[shCAMKK1] were separately dissolved in saline solution and administered to the mice i.v. for 4 weeks. As a control, equivalent volumes of PBS were injected. Body weight was monitored every week throughout the experiment. Mice (n = 6 in each group) were individually housed, and cumulative food intake in these animals was calculated as the difference between the amount of food given and the amount of food that remained every week during treatment. All animals were euthanised after overnight fasting (12 h) at the end of the study. Blood samples collected from the retinal vein plexus were centrifuged (3,500 rpm, 10 min, 4 °C) to separate the serum and then stored at -80 °C for further research. To calculate the liver index (liver weight/body weight) and relative weight of epididymal adipose tissue to body weight, the entire liver and epididymal adipose tissue was removed and weighed.

Histological analyses

Liver specimens were fixed in 10% formaldehyde solution for 24 h and prepared into 4-μm-thick sections after embedding in paraffin. To investigate the liver histopathological damage, each group's section areas were deparaffinised with xylene, rehydrated with ethanol solutions of different concentrations, and then dyed with H&E.

Oil Red O staining

Liver samples were frozen in optimal cutting temperature compound and sectioned. The sections of each group were dyed with Oil Red O (Sigma) to detect neutral lipid accumulation according to standard procedures. Briefly, tissue slices were dyed with 5% Oil Red O (in 60% isopropanol) at room temperature for 10 min. An upright fluorescence microscope (Nikon TE300, Tokyo, Japan) was used to observe the oil droplet images at 400 × magnification.

Hepatic lipid extraction and biochemical analyses

The same portion of liver tissues was excised from all mouse groups to extract liver lipids. Lipid extraction reagent was prepared with chloroform, methanol, and PBS at an 8:4:3 ratio. Then 75-mg liver tissues were mixed thoroughly with lipid extraction reagent overnight at 4 °C. After 12 h of incubation, the mixture was centrifuged at 3,000 rpm for 20 min at 4 °C. The lower organic phase was aspirated, and the samples were evaporated under nitrogen flow and resuspend in 200 μl methanol. The levels of serum alanine transaminase (ALT), aspartate transaminase (AST), triglycerides (TG), total cholesterol (TC), and liver TG. TC was investigated using the ADVIA 2400 Chemical System (Siemens, Tarrytown, NY, USA) following the manufacturer's instructions.

Glucose and insulin tolerance tests

Blood glucose levels were monitored at time points as indicated. For the insulin tolerance test (ITT), mice fasted for 6 h, and insulin (0.75 units/kg; Humulin R, Eli Lilly, Indianapolis, IN, USA) was administered i.p. The i.p. glucose tolerance test (IPGTT) was performed at the end of the study; mice fasted for 16 h, and glucose was then injected i.p. (1 g/kg body weight). The AUC of glucose was calculated during the course of the tests.

Nile red staining

Nile red (1 mg/ml) (Sigma) was prepared in an acetone solution. To visualise lipid droplets, 4% paraformaldehyde-fixed cells were dyed with 0.5 μg/ml Nile red (1:3,000 dilution) for 5 min, followed by PBS washing and DAPI staining after being fixed with 4% paraformaldehyde.[22] Fluorescence was determined using CytationTM5 (BioTek, Winooski, VT, USA) and quantified for five random areas using ImageJ 7.0 software.

FDA and cell viability assay

L02 was seeded at a density of 5.0×10^5/well and exposed to 2.0 mM OPA combined with different concentrations of MSC-ex for 24 h. PBS- or deMSC-ex-treated L02 was used as a control. L02 was cultured in a medium supplemented with 10 μM fluorescein diacetate (FDA) at 37 °C for 20 min. Finally, the cell viability of MSC-ex-treated L02 was detected by the Cytation 5 Imaging Reader (Biotek). There were three replicates per group. For the cell viability assay, Cell Counting Kit-8 (CCK-8, Vazyme, Nanjing, Jiangsu, China) was used to evaluate the proliferation of L02 cells as per the manufacturer's protocol. The assay was repeated thrice.

mRNA-seq and non-targeted lipidomics analyses

L02 was seeded at a density of 5.0×10^5/well and exposed to 2.0 mM OPA combined with MSC-ex (800 μg/ml) for 24 h. PBS-

treated L02 was used as a control. Then the cells and total RNA were collected for mRNA sequencing (mRNA-seq) and non-targeted lipidomics analyses. Specifically, mRNA-seq analyses included a normal hepatocyte group (normal, n = 3), a lipotoxic hepatocyte group (PBS, n = 3), and an MSC-ex treatment group (800 μg/ml, n=3). The non-targeted lipidomics analyses included a normal hepatocyte group (normal, n = 6), a lipotoxic hepatocyte group (PBS, n = 6), and an MSC-ex treatment group (800 μg/ml, n = 6). mRNA-seq analyses on liver tissue were performed on HFD-fed mice treated with MSC-ex (10 mg/kg) or PBS for 4 weeks. Then the liver tissues and total RNA were collected for mRNA-seq. Gene Denovo Biotechnology Co., Ltd, Guangzhou, performed all sample sequencing analyses.

Fatty acid oxidation assay
L02 was seeded at a density of 5.0×10^5/well and exposed to 2.0 mM OPA combined with MSC-ex (800 μg/ml) for 24 h. PBS- or deMSC-ex-treated L02 was used as a control. L02 mitochondria were isolated using a Mitochondrial Isolation Kit (Beyontime, Shanghai, China), and the fatty acid β-oxidation rates in mitochondria were determined using a Fatty Acid β-Oxidation Kit following the manufacturer's instructions (GenMed Scientifics Int, Boston, MA, USA).[23]

Immunofluorescence staining
Liver tissue and cultured cells were fixed in 4% para-formaldehyde (>30 min, at 4 °C) and then ruptured with 0.1% Triton X-100 (dilution in PBS) and blocked with 5% bovine serum albumin. Liver tissue segments and cultured cells were incubated with anti-CAMKK1 (ABclonal; rabbit, polyclonal, 1:100), anti-p-AMPK (Bioworld; rabbit, polyclonal, 1:200), anti-PPARα (Proteintech; rabbit, polyclonal, 1:100), anti-CPT-1A (Proteintech; rabbit, polyclonal, 1:100), anti-SREBP-1C (Proteintech; rabbit, polyclonal, 1:100), anti-FASn (Santa Cruz; mouse, monoclonal, 1:200), anti-p-IRS1 (Invitrogen; rabbit, polyclonal, 1:100), and anti-CD81 (Abcam; mouse, monoclonal, 1:100). Then the slides were labelled with fluorescein isothiocyanate-conjugated goat anti-rabbit IgG (Invitrogen; 1:200) and Alexa Fluor 555-conjugated donkey anti-mouse IgG. The nuclei were stained with Hoechst33342 (Sigma; 1:200). The slides were observed under a confocal microscope (DeltaVision Elite, GE, Boston, MA, USA), and the images were analysed using ImageJ 7.0 software.

Plasmid construction and transfection
Plasmid vectors were constructed by Fenghui Shengwu Co., Ltd. (China). The full-length cDNA of the human CAMKK1 gene (NCBI Gene ID: NM_032294) was inserted into the pCDH-CMV-MCS-GFP+Puro plasmid vector (Amp resistance, EcoRI, and BamHI restriction sites) to construct an overexpression plasmid. An endotoxin-free plasmid small extraction kit was used for extraction and purification. The purified plasmid was amplified and identified by single enzyme digestion and agarose electrophoresis. To corroborate the effect and mechanism of MSC-ex-derived CAMKK1 on lipid metabolism, the vector control (pCtr) and pCAMKK1 plasmids (2 and 4 μg) were transiently transfected into L02 and 293T cells for 48 or 24 h using Lipo2000 transfection reagent (Invitrogen) based on the manufacturer's instructions. Then L02 and 293T cells were incubated with 2.0 mM OPA for 24 h. Total RNA and protein were extracted for subsequent experiments. To further evaluate whether AMPK

activation is essential for the inhibitory effect of CAMKK1 on lipid accumulation, the vector control and pCAMKK1 plasmids (4 μg) were transiently transfected into L02 and 293T cells for 48 and 24 h. Then the cells were exposed to 2.0 mM OPA with or without compound C (2 and 4 μM) for 24 h. Cells from each group were collected to extract protein or total RNA for subsequent experiments.

### Quantitative reverse transcription PCR
The total RNA of cultured cells was isolated with TRIzol reagent (Invitrogen) and 1 μg RNA was reverse-transcribed to cDNA with an RNeasy kit (QIAGEN, Hilden, Germany). Quantitative reverse transcription PCR (QRT-PCR) was carried out using the ABI Prism 2720 PCR system (Applied Biosystems, Boston, MA, USA); the relative mRNA expression was measured using the $2^{-\Delta\Delta Ct}$ method, and β-ACTIN was used as a control. The following primers were used: Homo-CAMKK1, 5′-CATCAAGCCATC-CAACCTG-3′ (forward); 5′-CTC CTC TGT CAC CTC CAC C-3′ (reverse); Homo-tumour necrosis factor (TNF)-α, 5′-CCT CTC TCT AAT CAG CCC TCT G-3′ (forward); 5′-GAG GAC CTG GGA GTA GAT GAG-3′ (reverse); Homo-IL-1β, 5′-TGT ACC TGT CCT GCG TGT TG-3′ (forward); 5′-GCC CTA GGG ATT GAG TCC AC-3′ (reverse); Homo-IL-6, 5′-ACT CAC CTC TTC AGA ACG AAT TG-3′ (forward); 5′-CCA TCT TTG GAA GGT TCA GGT TG-3′ (reverse); Homo-β-ACTIN, 5′-GAC CTG TAC GCC AAC ACA GT-3′ (forward); 5′-GAT AAG CCG TGG TTC TGG TC-3′ (reverse); and Mus-CAMKK1, 5′-TGC TGT CTG TGG GAC TGC ATA-3′ (forward); 5′- GGA TCC ACA CCA TTC CTG GC-3′ (reverse); Mus-TNF-α, 5′-CAT CTT CTC AAA ATT CGA GTG ACA A-3′ (forward); 5′-TGG GAG TAG ACA AGG TAC AAC CC-3′ (reverse); Mus-IL-1β, 5′-CCG TGG ACC TTC CAG GAT GA-3′ (forward); 5′-GGG AAC GTC ACA CAC CAG CA-3′ (reverse); Mus-IL-6, 5′-AGT TGC CTT CTT GGG ACT GA-3' (forward); 5′-TCC ACG ATT TCC CAG AGA AC-3′ (reverse); Mus-β-ACTIN, 5′-GTG ACG TTG ACA TCC GTA AAG A-3′ (forward); 5′-GCC GGA CTC ATC GTA CTC C-3′ (reverse).

Lentiviral knockdown of CAMKK1 in MSCs
The lentiviral vector containing CAMKK1 short hairpin RNA (shRNA) sequence (pLKO.1-GFP-Puro-shCAMKK1; Vigen Biotech, Shanghai, China) was explicitly designed to target CAMKK1 silencing; a negative control vector (pLKO.1-Puro-shRNA) was also prepared. CAMKK1 shRNA (sequence: GCTGAGGA-CAACCTCTATTTG) and control shRNA (non-targeting) oligonucleotides were inserted into the pLKO.2-U6-MSC-hPGK-copGFP-puro lentiviral vector to generate CAMKK1 and control green fluorescent protein (GFP)-labelled shRNA expression vectors. After the virus was prepared, MSCs were transduced with recombinant lentivirus (pLKO) (pLKO.1-GFP-Puro-shCAMKK1 or pLKO.1-Puro-shRNA, 25 multiplicity of infection). Transduced MSCs were screened with 1 mg/ml puromycin (Sigma) for 12 days to obtain stable cell lines. Then shRNA expression in MSCs was induced with 80 μg/ml doxycycline, and immunoblotting analyses and QRT-PCR confirmed knockdown efficiency. Stable cell line (MSC[shCtr] and MSC[shCAMKK1]) for the collection of MSC-ex[shCtr] and MSC-ex[shCAMKK1].

Statistical analyses
All experiments (including cell and mouse-based experiments) included biological replicates and were repeated at least three times. The data represent the mean ± SEM. The Pearson
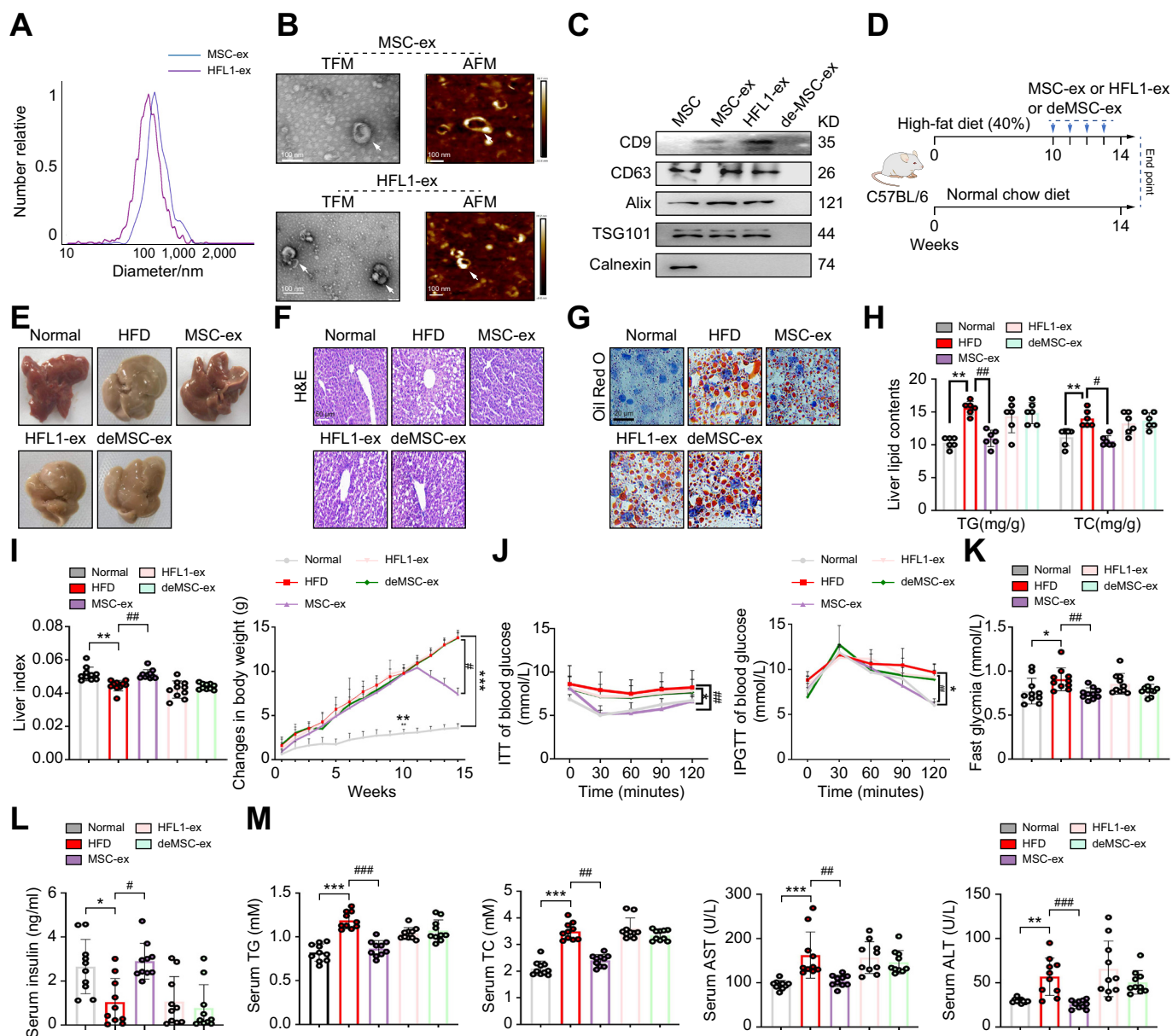
Fig. 1. Therapeutic efficacy of MSC-ex in the HFD-induced NAFLD model. (A) Representative result of NTAs of MSC-ex and HFL1-ex. (B) Representative results of nanosized vesicles (MSC-ex and HFL1-ex) photographed by TEM and AFM. Scale bar, 100 nm. (C) Exosome markers CD9, CD63, Alix, and TSG101 were positive in MSC-ex and HFL1-ex by immunoblotting. (D) C57BL/6 mice were fed a HFD (40%) for 10 weeks and then were i.v. administered PBS as a control or 10 mg/kg MSC-ex or 10 mg/kg HFL1-ex or deMSC-ex from the 10th week to the 14th week of HFD feeding. (E) Representative Images of gross liver appearance from mice. (F and G) Representative images of H&E (scale bars, 50 μm) (F) and Oil Red O (scale bars, 20 μm) staining (G) of liver sections from mice from each treatment group. (H) Liver contents of total TG and TC in each group. (I) Liver indexes (liver index = liver wet weight/body weight) and body weight changes of mice from each group. (J) i.p. ITTs evaluated individual insulin tolerance by injecting insulin at a dose of 0.75 IU/kg body weight; blood glucose levels were detected at 0, 30, 60, 90, and 120 min and compared with that at 0 min. Individual glucose tolerance was assessed by IPGTT; fasted mice were administered 1 g of glucose/kg body weight by i.p. injection, and blood glucose levels were determined at 0, 30, 60, 90, and 120 min. (K) Fasting glycaemia (after 16-h fast). (L and M) Serum insulin (L), and TG, TC, AST, and ALT (M) levels in each group. Data are represented as the mean ± SEM. Statistical analyses were performed by a one-way ANOVA (H–M). *p <0.05, **p <0.01, ***p <0.001 *vs.* normal chow diet group; #p <0.05, ##p <0.01, ###p <0.001 *vs.* HFD group. AFM, atomic force microscopy; ALT, alanine transaminase; AST, aspartate transaminase; deMSC-ex, MSC-ex-free conditional medium supernatant; HFD, high-fat diet; HFL1, human lung fibroblast 1; HLF1-ex, foetal HFL1-derived exosomes; IPGT, i.p. glucose tolerance test; ITT, insulin tolerance test; MSC-ex, MSC-derived exosomes; MSC, mesenchymal stem cell; NAFLD, non-alcoholic fatty liver disease; NTA, nanoparticle tracking analysis; TC, total cholesterol; TFM, transmission electron microscopy; TG, triglycerides; TSG101, tumour susceptibility gene 101.

normality test and D'Agostino test were used to determine the normal distribution. Prism 8 software (GraphPad, San Diego, CA, USA) was used to analyse variance or t tests to evaluate statistically significant differences between groups. All statistical tests were two-tailed, and p <0.05 was defined as significant.

Ethics approval and patient consent statement
All experiments involving animals were conducted according to the ethical policies and procedures approved by the Jiangsu University Ethics Committee (approval no. UJS-IACUC-AP-2020033127). The use of human umbilical cord tissues
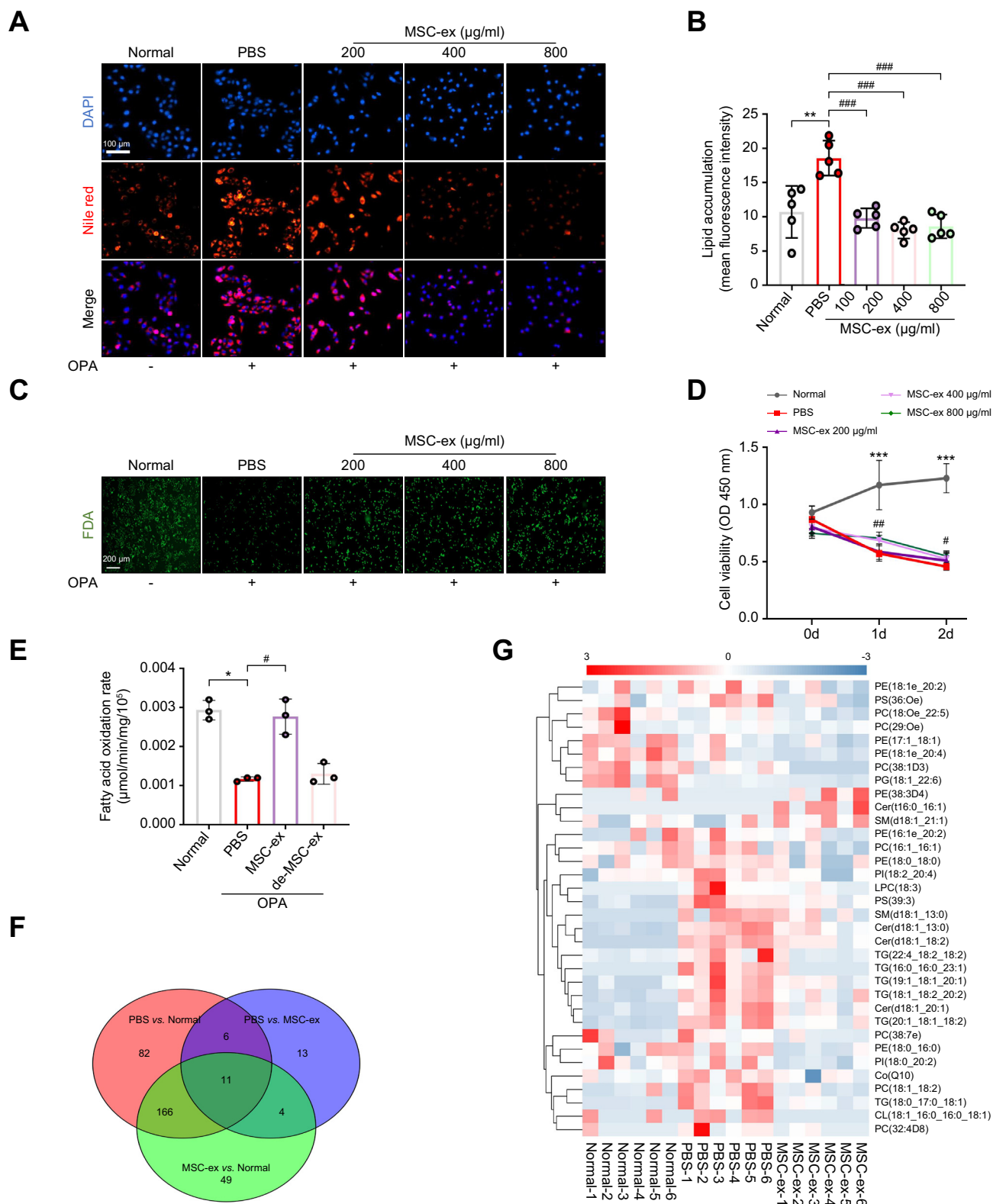
Fig. 2. MSC-ex inhibit lipid accumulation *in vitro* by promoting the β-oxidation of fatty acids and suppressing the fatty acid synthesis. (A and B) Intracellular lipid droplets in L02 cells stimulated with OPA (2.0 mM, 2:1 ratio) in combination with different concentrations of MSC-ex or PBS for 24 h were visualised by Nile red staining (A) and quantified by ImageJ for five random areas (B). Scale bars, 100 μm. (C) Cell viability was measured by FDA staining. (D) The effect of MSC-ex on the viability of L02 cells was determined by CCK-8 assay. (E) Mitochondrial fatty acid β-oxidation of L02 cells treated with a combination of OPA and MSC-ex (800 μg/ml) or deMSC-ex for 24 h, n = 3 biological replicates per group. (F and G) Lipogenic metabolites in L02 cells subjected to stimulation with OPA (2.0 mM, 2:1 ratio) combined with MSC-ex (800 μg/ml) or PBS treatment for 24 h were observed by non-targeted lipidomics (n = 6 per group), followed by Venn diagram (F) and heat map (G) analyses of fatty acid metabolites. Data are represented as mean ± SEM. Statistical analyses by a one-way ANOVA (B, D, and E). $*p$ <0.05, $**p$ <0.01, $***p$ <0.001 *vs.* normal group; $^{#}p$ <0.05, $^{##}p$ <0.01, $^{###}p$ <0.001 *vs.* PBS group. CCK-8, Cell Counting Kit-8; deMSC-ex, MSC-ex-free conditional medium supernatant; FDA, fluorescein diacetate; MSC-ex, MSC-derived exosomes; MSC, mesenchymal stem cell; OPA, oleate and palmitate.

was approved by the Jiangsu University Ethics Committee (2012258).

Results

MSC-ex administration ameliorates liver steatosis in the HFD-induced NAFLD mice

According to the guideline of the International Society for Extracellular Vesicles,[24] MSC-ex isolated from MSC-conditioned medium and HFL1-ex isolated from HFL1-conditioned medium were characterised in terms of size, morphology, and surface markers. Nanoparticle tracking analyses indicated that the mean diameter of MSC-ex and HFL1-ex was approximately 110 nm (Fig. 1A). Furthermore, TEM and AFM analyses confirmed that MSC-ex and HFL1-ex had a characteristic lipid bilayer (Fig. 1B), and immunoblotting analyses confirmed that MSC-ex and HFL1-ex were positive for exosome markers, including CD9, CD63, Alix, and TSG101, whereas the endoplasmic reticulum protein calnexin was not detected (Fig. 1C).
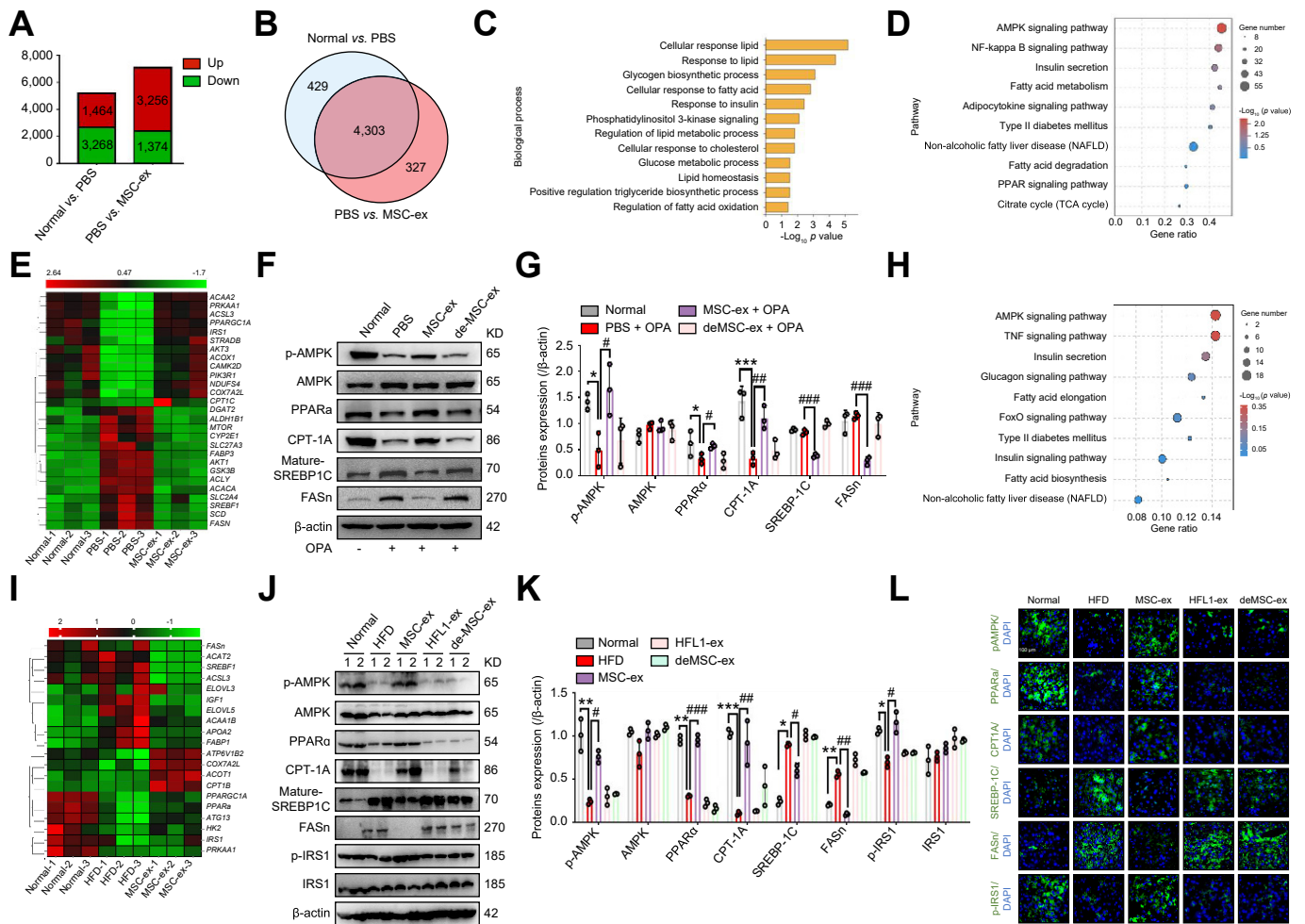
Fig. 3. MSC-ex activate AMPK-mediated PPARα/CPT-1A and the SREBP-1C/FASn signalling pathway in hepatocytes and liver tissues. (A and B) mRNA-seq analyses were performed on L02 cells that were untreated (normal group) or subjected to OPA stimulation (2.0 mM, ratio of 2:1) combined with MSC-ex (800 μg/ml) (MSC-ex group) or PBS treatment (PBS group) for 24 h, n = 3 biological replicates per group. Histogram (A) and Venn diagram (B) analyses of differentially expressed genes. (C) Gene ontology analyses of differentially activated biological processes. (D) The top 10 enriched pathways as determined by the KEGG database. (E) Heat map of differentially expressed genes in the AMPK signalling pathway. (F and G) Evaluation of protein expression by immunoblotting (F) and quantification of the results (G). n = 3 biological replicates per group; *p <0.05, ***p <0.001 *vs.* normal group; #p <0.05, ##p <0.01, ###p <0.001 *vs.* PBS group. (H and I) mRNA-seq analyses were performed on liver tissues in mice placed on a HFD for 10 weeks followed by 10 mg/kg MSC-ex or PBS treatment for 4 weeks. n = 3 biological replicates per group. The top 10 enriched pathways as determined by the KEGG database (H) and heatmap (I) of differentially expressed genes in the AMPK signalling pathway. (J and K) Immunoblotting analyses of AMPK signalling proteins in mice placed on a HFD for 10 weeks followed by 10 mg/kg MSC-ex or 10 mg/kg HFL1-ex or deMSC-ex and PBS treatment for 4 weeks (J) and quantification of the results (K). *p <0.05, **p <0.01, ***p <0.001 *vs.* normal chow diet group; #p <0.05, ##p <0.01, ###p <0.001 *vs.* HFD group. (L) Immunofluorescence images of staining for p-AMPK, PPARα, CPT-1A, SREBP-1C, FASn, and p-IRS1 (green) in liver sections of mice. Nuclei were labelled with DAPI (blue). Scale bars, 100 μm. Data are represented as the mean ± SEM. Statistical analyses by a one-way ANOVA (G and K). AMPK, AMP-activated protein kinase; CPT-1A, carnitine palmitoyltransferase 1A; deMSC-ex, MSC-ex-free conditional medium supernatant; FASn, fatty acid synthase; HFD, high-fat diet; HFL1-ex, foetal HFL1-derived exosomes; HFL1, human lung fibroblast 1; IRS1, insulin receptor substrate 1; KEGG, Kyoto Encyclopedia of Genes and Genomes; mRNA-seq, mRNA sequencing; MSC-ex, MSC-derived exosomes; MSC, mesenchymal stem cell; NAFLD, non-alcoholic fatty liver disease; OPA, oleate and palmitate; p-AMPK, phosphorylated AMPK; p-IRS1, phosphorylated IRS1; PPARα, peroxisome proliferator-activated receptor alpha; SREBP-1C, sterol regulatory element-binding protein-1C; TCA, tricarboxylic acid cycle; TNF, tumour necrosis factor.

To evaluate the therapeutic efficacy of MSC-ex in liver steatosis, we fed mice a HFD for 14 weeks. We administered deMSC-ex, MSC-ex, or HFL1-ex i.v. at a dose of 10 mg/kg weekly for 4 weeks, starting at week 10 after HFD feeding (Fig. 1D). Macroscopic inspection of livers revealed that the MSC-ex group was of near normal colour and appearance, whereas HFD, HFL1-ex, or deMSC-ex mice displayed pale yellow surfaces (Fig. 1E). H&E and Oil Red O staining revealed that MSC-ex-treated mouse livers displayed less vacuolisation and reduced accumulation of intracellular lipid droplets compared with HFL1-ex or deMSC-ex mice (Fig. 1F and G). MSC-ex did not affect hepatic lipid deposition in normal mice (Fig. S1A). Liver TG and TC levels in HFD-fed mice were also inhibited by MSC-ex administration (Fig. 1H). The liver index and body weight of the mice was measured once a week. Increased liver index and decreased body weight were found in mice fed with MSC-ex, compared with mice fed with HFL1-ex or deMSC-ex (Fig. 1I). MSC-ex administration also showed less weight gain of inguinal adipose tissue in HFD-fed mice (Fig. S1B). In contrast, food intake was not significantly altered between different groups, and this trend was sustained over the entire treatment period (Fig. S1C).

Peripheral insulin resistance is responsible for the pathogenesis of NAFLD. To examine whether MSC-ex affect the insulin sensitivity of mice to regulate blood glucose, we compared the ITT, IPGTT, fast blood glucose levels, and serum insulin levels of HFD mice between MSC-ex and other groups. Compared with results in the HFL1-ex or deMSC-ex groups, results of the ITT and IPGTT showed that MSC-ex were able to bring blood glucose levels back to normal quickly in insulin-and glucose-injected mice (Fig. 1J). Fasting blood glucose levels were also decreased and serum insulin levels were increased in MSC-ex mice (Fig. 1K and L). Furthermore, elevated liver damage markers such as serum TG, TC, ALT, and AST in the HFD group were reversed by MSC-ex but not by HFL1-ex and deMSC-ex (Fig. 1M). Expression of inflammatory factors TNF-α, IL-1, and IL-6 in the livers of HFD mice was also reduced by MSC-ex treatment (Fig. S1D). These findings indicate that MSC-ex treatment effectively prevents hepatic steatosis and improves liver function in HFD mice.

MSC-ex inhibit lipid accumulation *in vitro* by promoting the β-oxidation of fatty acids and suppressing the fatty acid synthesis

Lipid metabolism disorder contributes to lipid accumulation in hepatocytes and plays a vital role in the pathogenesis of liver steatosis. To explore the underlying mechanisms by which MSC-ex attenuate hepatic steatosis, we assessed the effect of MSC-ex on lipid metabolites in OPA-treated L02 human hepatocyte cells. PBS and HFL1-ex were used as controls. MSC-ex and HFL1-ex could be located in the cytoplasm of OPA-L02 cells at 12 h post incubation (Fig. S2A and B). Nile red staining showed that MSC-ex treatment significantly decreased hepatocyte lipid accumulation in a dose-dependent manner (Fig. 2A and B). FDA staining and CCK-8 assay revealed that OPA-reduced cell viability was increased by MSC-ex (Fig. 2C and D), whereas HFL1-ex showed no effect on lipid accumulation (Fig. S2C and D). Given the critical roles of lipid metabolic pathways in hepatocytes, we investigated the effects of MSC-ex on fatty acid oxidation and metabolite production in OPA-treated L02 cells. As shown in Fig. 2E, MSC-ex treatment significantly increased the fatty acid β-oxidation rate compared with that in control groups treated with

PBS or deMSC-ex. To further understand the lipid metabolite changes that occur during MSC-ex treatment, OPA-L02 was treated with PBS or MSC-ex (800 μg/ml) for 24 h, and then liquid chromatography–mass spectrometry (LC-MS)-based non-targeted lipidomic analyses were performed. Changes in lipid metabolites were evaluated using the Venn diagram and heat map cluster analyses using R package ropls tools (University of Auckland, New Zealand). Among 331 lipids examined, a total of 34 lipid molecules changed significantly in the MSC-ex group compared with the PBS group, of which 31 (91.18%) were reduced by MSC-ex (Fig. 2F and G). These findings suggest that MSC-ex treatment increases the fatty acid β-oxidation rate and reduces the production of lipid metabolites, which provides additional evidence for the role of MSC-ex in reducing lipid accumulation by promoting β-oxidation of fatty acids and suppressing fatty acid synthesis.

MSC-ex activate AMPK-mediated PPARα/CPT-1A and the SREBP-1C/FASn signalling pathway

To clarify the mechanisms underlying the regulation by MSC-ex of lipid metabolism, we evaluated differentially expressed genes in untreated and OPA-treated L02 cells from the PBS and MSC-ex groups using mRNA-seq. A total of 4,630 genes (3,256 upregulated, 1,374 downregulated) were differentially expressed between the PBS and MSC-ex groups (Fig. 3A), and 4,303 of these were also differentially expressed between the untreated (normal) and PBS groups (Fig. 3B). Among these 4,303 genes, gene ontology analyses for biological processes identified multiple terms associated with lipid metabolism (Fig. 3C), supporting our observations that MSC-ex regulate lipid homoeostasis. Furthermore, Kyoto Encyclopedia of Genes and Genomes (KEGG) pathway analyses revealed the enrichment of multiple metabolic pathways, including the AMPK pathway, which was the most highly enriched signalling pathway and was upregulated in the MSC-ex group (Fig. 3D). Given the dominant role of AMPK in liver lipid metabolism, we performed unsupervised hierarchical clustering for AMPK-regulated fatty acid synthesis and fatty acid oxidation genes and observed consistent trends of modulation (Fig. 3E).

Emerging evidence has suggested that the AMPK-regulated SREBP-1C/FASn and PPARα/CPT-1A play crucial roles in the regulation of lipid metabolism in NAFLD. FASn is a critical lipogenic enzyme in NAFLD owing to its ability to promote hepatic fatty acid synthesis.[25] PPARs, which are nuclear receptors that regulate fatty acid oxidation by CPT-1A, act as critical players in lipid catabolism, and hepatic PPARα is decreased in patients with NAFLD.[26] Therefore, we evaluated AMPK activation and AMPK-regulated gene expression in MSC-ex-treated OPA-L02 cells. As shown in Fig. 3F and G, MSC-ex treatment enhanced the expression of p-AMPK, PPARα, and CPT-1A and inhibited the expression of mature-SREBP-1C and FASn in OPA-L02, when compared with the levels in the PBS group.

mRNA-Seq differential expression analysis of livers from MSC-ex- and PBS-treated HFD mice also revealed the similar effect of MSC-ex on AMPK-regulated fatty acid synthesis and fatty acid oxidation genes at the cellular level *in vitro* (Fig. 3H and I). Compared with those in the HFL1-ex or deMSC-ex group, increased p-AMPK, PPARα, and CPT-1A, and reduced mature-SREBP-1C and FASn expression were shown in the MSC-ex group (Fig. 3J–L), which was not found in HFL1-ex group
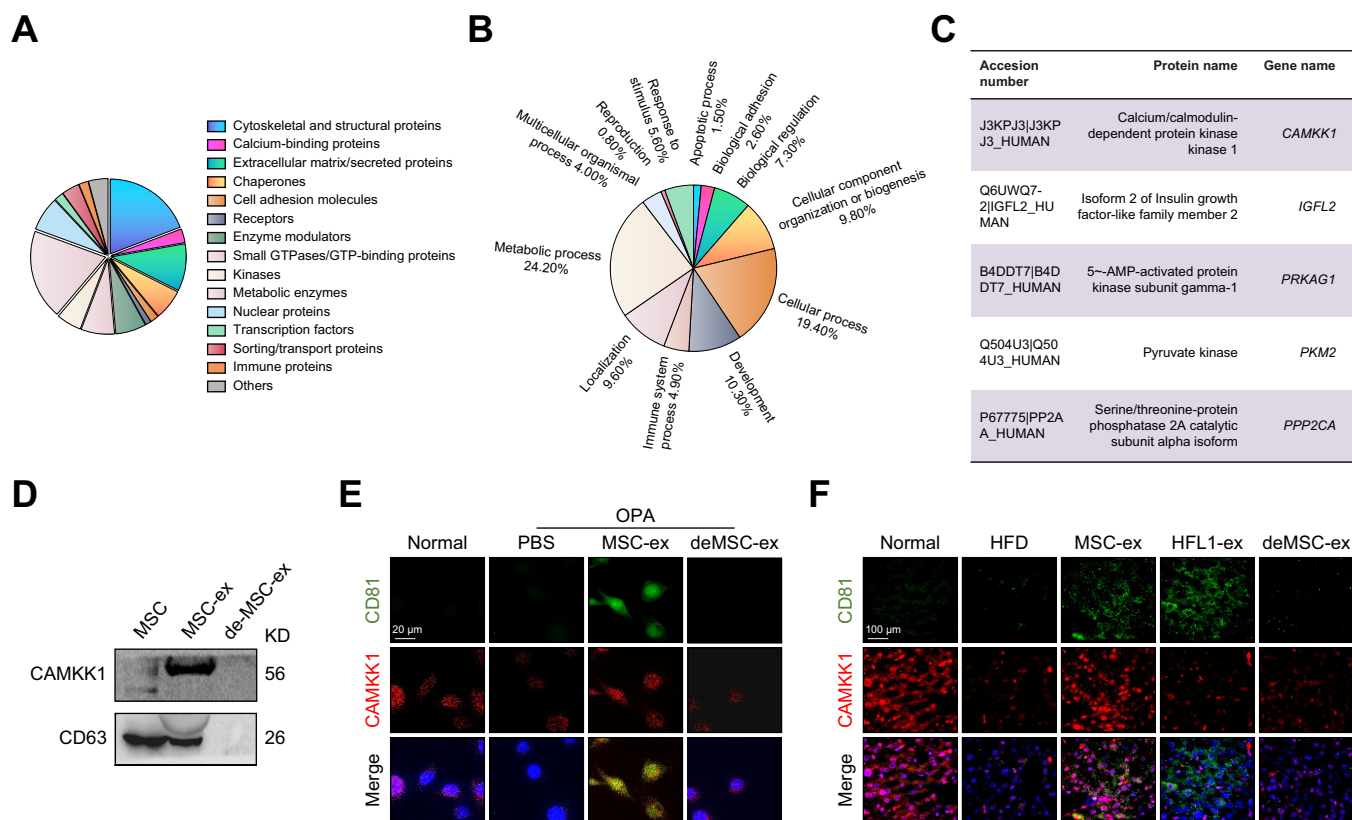
Fig. 4. MSC-ex transport CAMKK1 into liver tissues and hepatocytes. (A and B) Proteomic profiling of MSC-ex as compared with HFL1-Ex was analysed by LC-MS/MS. (A) Protein classification diagram and (B) Biological process enrichment analyses. (C) A partial list of proteins involved in metabolic biological processes. (D) CAMKK1 expression in MSC-ex was examined by immunoblotting. (E and F) Representative confocal microscopy images of CD81 (green) and CAMKK1 (red) colocalisation in L02 cells subjected to OPA stimulation (2.0 mM, 2:1 ratio) in combination with MSC-ex (800 μg/ml), deMSC-ex, or PBS treatment for 24 h (E) and liver sections of mice fed a normal chow diet (n = 10) or HFD and injected with PBS (n = 10), 5 mg/kg MSC-ex (n = 10), or 10 mg/kg MSC-ex (n = 10) (F); nuclei were labelled with DAPI (blue). Scale bars, 20 μm. CAMKK1, calcium/calmodulin-dependent protein kinase 1; de-MSC-ex, MSC-ex-free conditional medium supernatant; HFD, high-fat diet; HFL1-ex, foetal HFL1-derived exosomes; HFL1, human lung fibroblast 1; LC-MS/MS, liquid chromatography–tandem mass spectrometry; MSC-ex, MSC-derived exosomes; MSC, mesenchymal stem cell; OPA, oleate and palmitate.

(Fig. S2E and F). Moreover, MSC-ex treatment also enhances the expression of insulin resistance marker p-IRS1 (Fig. 3J–L). These data suggest that MSC-ex-activated AMPK may promote fatty acid oxidation by upregulating the PPARα/CPT-1A pathway and reduce fatty acid synthesis by downregulating the SREBP-1C/FASn pathway.

MSC-ex-delivered CAMKK1 attenuates lipid accumulation in hepatic cells by activating the AMPK pathway

To explore which MSC-ex components confer anti-hepatic steatosis effects, we analysed the protein profile in MSC-ex using LC-MS/MS.[27] Approximately 24.2% of the proteins represented in the MSC-ex profile were involved in metabolic biological processes (Fig. 4A and B), suggesting that MSC-ex may regulate fatty acid homoeostasis by delivering metabolism-related enzymes. Interestingly, CAMKK1 was enriched in MSC-ex but not in deMSC-ex or HFL1-ex (Fig. 4C and D, and Fig. S3A). Consistently, CAMKK1 colocalised with the exosomal marker CD81 in hepatocytes after *in vitro* and *in vivo* MSC-ex exposure (Fig. 4E and F). We exam-

ined the mRNA and protein levels of CAMKK1 in OPA-L02, OPA-treated mouse hepatocyte AML12 (OPA-AML12), and steatotic livers before and after MSC-ex treatment. The level of CAMKK1 mRNA remained unchanged (Fig. S3B), and CAMKK1 protein in OPA-L02, OPA-AML12, and steatotic livers were increased after MSC-ex treatment (Fig. S3C–H). Immunoblotting results using an antimouse CAMKK1 antibody (N-terminal) showed that the CAMKK1 protein of mouse origin was not significantly affected by MSC-ex (Fig. S3E–H). In addition, PRKAG1 and IGFL2 were detected in MSC-ex but not in HFL1-ex (Fig. S3A), and the levels of PRKAG1 and IGFL2 protein were not changed in MSC-ex-treated OPA-L02 cells and OPA-AML12 cells (Fig. S3C–F).

Previous studies have reported that CAMKK1 activates AMPK in a Ca^{2+}-dependent manner in neural tissue.[28] However, the role of CAMKK1 in AMPK activation and lipid metabolism regulation in liver steatosis remains unknown. Thus, to corroborate the effect and mechanism of MSC-ex-derived CAMKK1 on lipid metabolism, we examined the regulation by CAMKK1 of AMPK activation and lipid metabolism in OPA-treated L02 and 293T
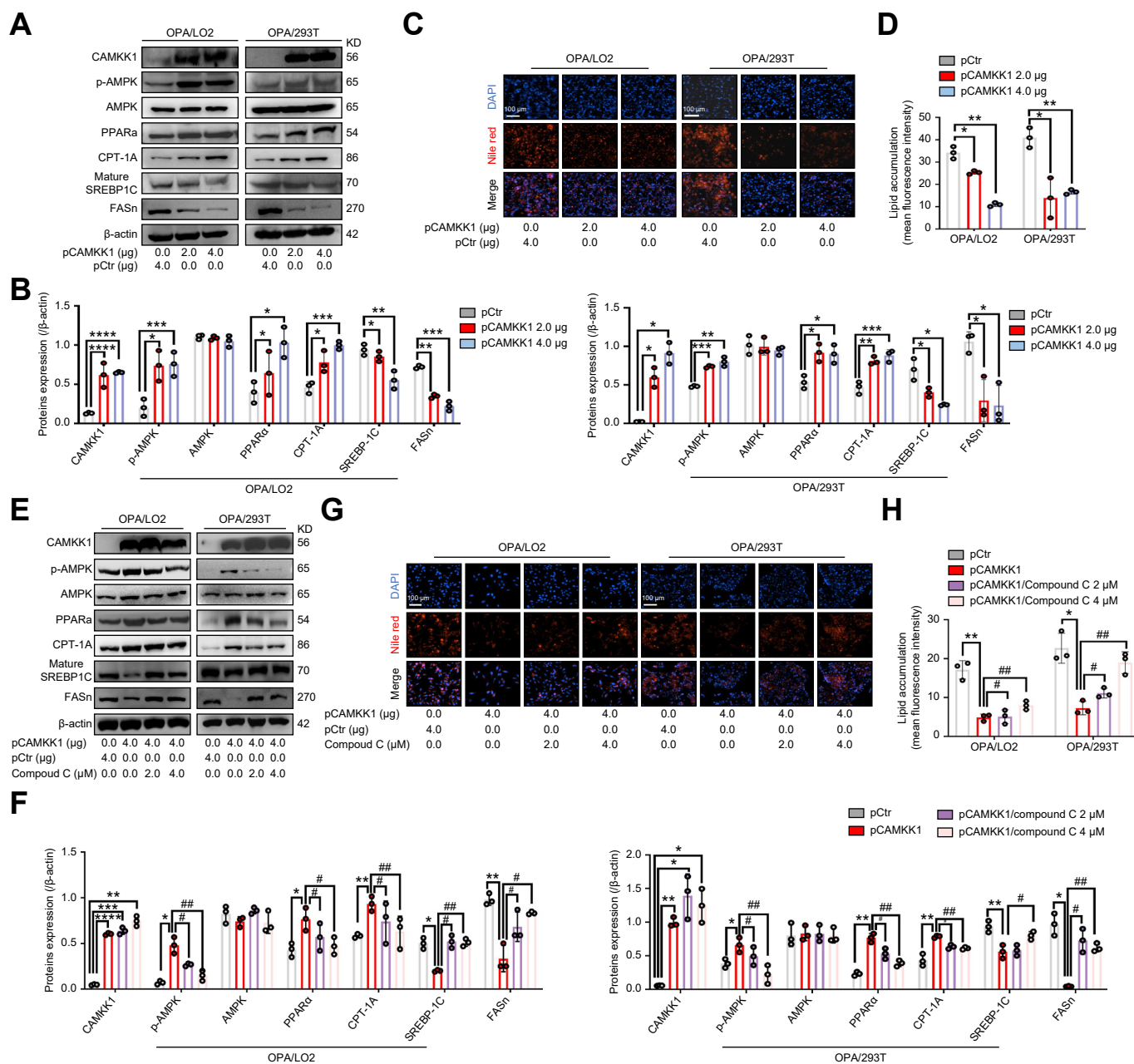
Fig. 5. Overexpression of CAMKK1 activates the AMPK signalling pathway and attenuates lipid accumulation in OPA-treated L02 and 293T cells. (A and B) The expression of AMPK signalling proteins in L02 and 293T cells transfected with pCAMKK1 (2 and 4 μg) or pCtr control vector before OPA stimulation (2.0 mM, 2:1 ratio) for 24 h was detected by immunoblotting (A) and quantified (B). (C and D) Intracellular lipid droplets in L02 and 293T cells were visualised by Nile red staining (C) and quantified by ImageJ for five random areas (D). Scale bars, 100 μm. (E and F) The expression of AMPK signalling proteins in L02 and 293T cells after transfection with pCAMKK1 (4 μg) or pCtr vector and OPA stimulation (2.0 mM, 2:1 ratio) with or without compound C (2 and 4 μM) treatment for 24 h was examined by immunoblotting (E) and quantified (F). (G and H) Intracellular lipid accumulation was visualised by Nile red staining (G) and quantified by ImageJ for three random areas (H). Data are represented as the mean ± SEM. Statistical analyses by unpaired two-tailed Student's *t* test (B and D) and a one-way ANOVA (F and H). *p <0.05, **p <0.01, ***p <0.001, ****p <0.0001 *vs.* pCtr group; #p <0.05, ##p <0.01 *vs.* pCAMKK1 (4 μg) group. AMPK, AMP-activated protein kinase; CAMKK1, calcium/calmodulin-dependent protein kinase 1; CPT-1A, carnitine palmitoyltransferase 1A; FASn, fatty acid synthase; OPA, oleate and palmitate; p-AMPK, phosphorylated AMPK; PPARα, peroxisome proliferator-activated receptor alpha; SREBP-1C, sterol regulatory element-binding protein-1C.

cells. Transfection of pCAMKK1 led to dose-dependent induction of p-AMPK, PPARα, and CPT-1A expression and reduction of mature-SREBP-1C and FASn expression compared with the levels in cells transfected with the vector control (pCtr) (Fig. 5A and B,

and Fig. S4A). In addition, transfection of pCAMKK1 resulted in a significant reduction of lipid accumulation in OPA-L02 and OPA-293T, as assessed by Nile red staining (Fig. 5C and D). We next evaluated the role of AMPK inhibition in pCAMKK1-induced
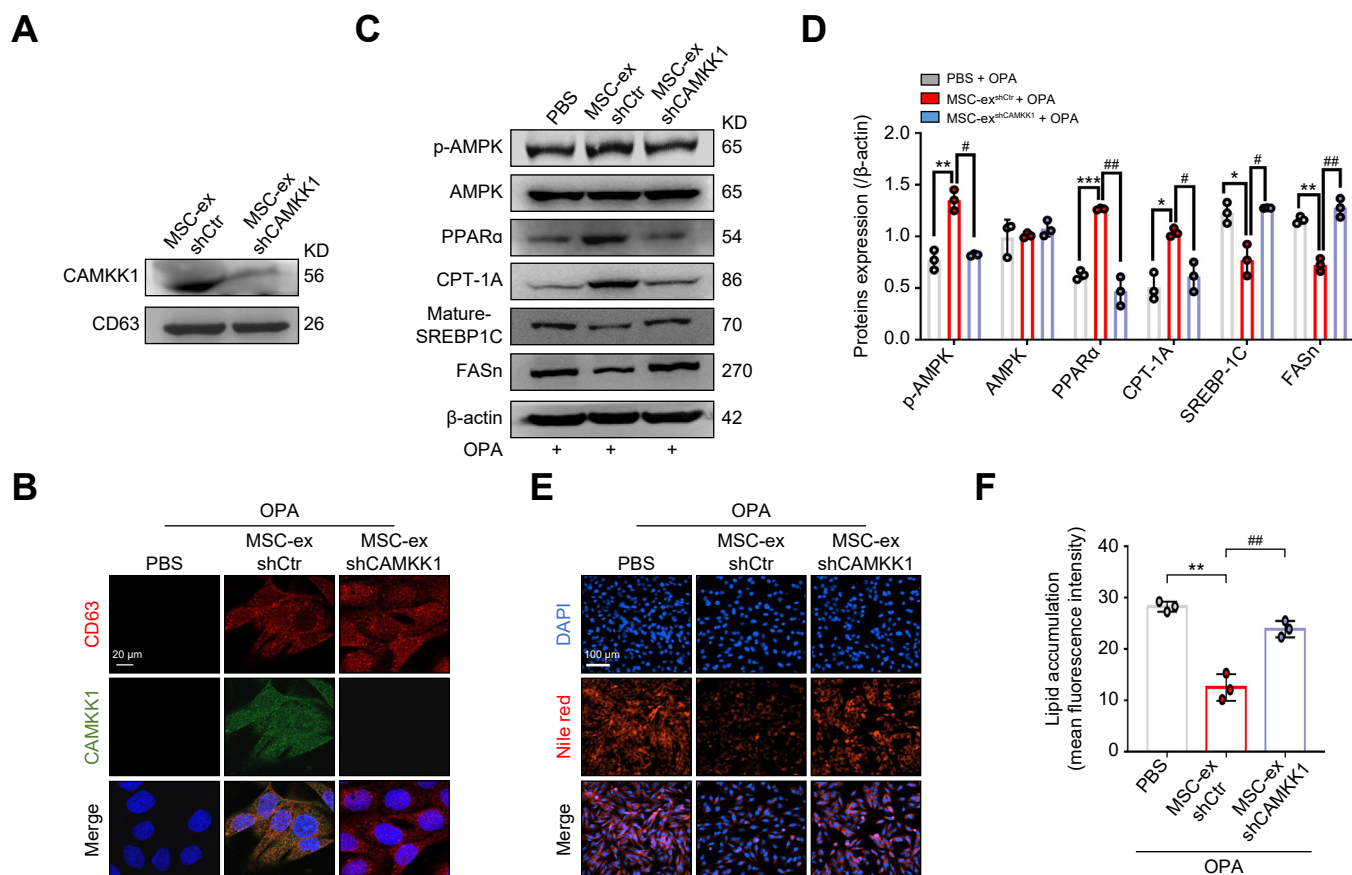
Fig. 6. Knockdown of CAMKK1 in MSC-ex inactivates the AMPK signalling pathway and increases lipid accumulation. (A) CAMKK1 expression in MSC-ex[shCtr] and MSC-ex[shCAMKK1] was examined by immunoblotting. (B) Representative confocal microscopy images of CD63 (red) and CAMKK1 (green) colocalisation in L02 cells treated with OPA in combination with PBS, MSC-ex[shCtr], or MSC-ex[shCAMKK1]; nuclei are labelled with DAPI (blue). Scale bars, 20 μm. (C and D) The expression of AMPK signalling proteins in L02 cells stimulated with OPA (2.0 mM, 2:1 ratio) and PBS, MSC-ex[shCtr] (800 μg/ml), or MSC-ex[shCAMKK1] (800 μg/ml) for 24 h was detected by immunoblotting (C) and quantified (D). (E and F) Intracellular lipid droplets in L02 cells were visualised by Nile red staining (E) and quantified by ImageJ for three random areas (F). Scale bars, 100 μm. Data are represented as the mean ± SEM. Statistical analyses by a one-way ANOVA (D and F). $^*p <0.05$, $^{**}p <0.01$, $^{***}p <0.001$ *vs.* PBS group; $^{#}p <0.05$, $^{##}p <0.01$ *vs.* MSC-ex (800 μg/ml) group. AMPK, AMP-activated protein kinase; CAMKK1, calcium/calmodulin-dependent protein kinase 1; CPT-1A, carnitine palmitoyltransferase 1A; FASn, fatty acid synthase; MSC-ex, MSC-derived exosomes; MSC, mesenchymal stem cell; OPA, oleate and palmitate; p-AMPK, phosphorylated AMPK; PPARα, peroxisome proliferator-activated receptor alpha; SREBP-1C, sterol regulatory element-binding protein-1C.

AMPK/PPARα/CPT-1A signalling and AMPK/SREBP-1C/FASn signalling. Compound C (an inhibitor of AMPK, 4 μM) blocked the activation of p-AMPK/PPARα/CPT-1A signalling and reduction of SREBP-1C/FASn signalling (Fig. 5E and F) but had no observable effects on CAMKK1 mRNA expression (Fig. S4B). Consistently, compound C diminished the inhibition of pCAMKK1 transfection in lipid accumulation (Fig. 5G and H).

CAMKK1 knockdown attenuates MSC-ex regulation of the AMPK pathway and lipid accumulation in OPA-L02 cells

To verify the role of CAMKK1 in MSC-ex-mediated regulation of lipid accumulation in hepatocytes, we generated CAMKK1 knockdown MSC-ex (MSC-ex[shCAMKK1]) by the transduction of a lentivirus carrying specific shRNA of CAMKK1 (lenti-shCAMKK1) in MSC. Effective knockdown was confirmed in MSC-ex[shCAMKK1] compared with MSC-ex[shCtr] (Fig. 6A). CAMKK1 colocalised with the exosomal marker CD63 in hepatocytes after *in vitro* MSC-ex exposure and abolished by CAMKK1 knockdown in MSC-ex by immunofluorescence staining (Fig. 6B). Increased p-AMPK, PPARα, CPT-1A expression and reduced mature-SREBP-1C and

FASn expression in OPA-L02 cells upon MSC-ex treatment was reversed by CAMKK1 knockdown (Fig. 6C and D). Furthermore, CAMKK1 knockdown abolished the MSC-ex-mediated reduction of lipid accumulation in OPA-L02 cells (Fig. 6E and F). To further elucidate the species specificity of the lenti-shCAMKK1, we compared the silence effect of lenti-shCAMKK1 in L02 cells and AML12 cells. Lenti-shCAMKK1 decreased mRNA and protein expression of CAMKK1 in L02 cells (Fig. S5A and B), which was not found in AML12 cells (Fig. S5C and D). In addition, CAMKK1 knockdown of MSC-ex with lenti-shCAMKK1 did not affect CAMKK1 mRNA expression in either the L02 or AML12 cells (Fig. S5E and F). These results demonstrate that CAMKK1 plays an essential role in MSC-ex-mediated AMPK activation and lipid accumulation reduction.

CAMKK1 knockdown attenuates MSC-ex regulation of the AMPK pathway and hepatic steatosis in NAFLD mice

To evaluate the role of CAMKK1 in NAFLD mice, we administered MSC-ex[shCtr] and MSC-ex[shCAMKK1] (10 mg/kg) i.v. into HFD mice weekly for 4 weeks (Fig. 7A). CAMKK1 protein expression was
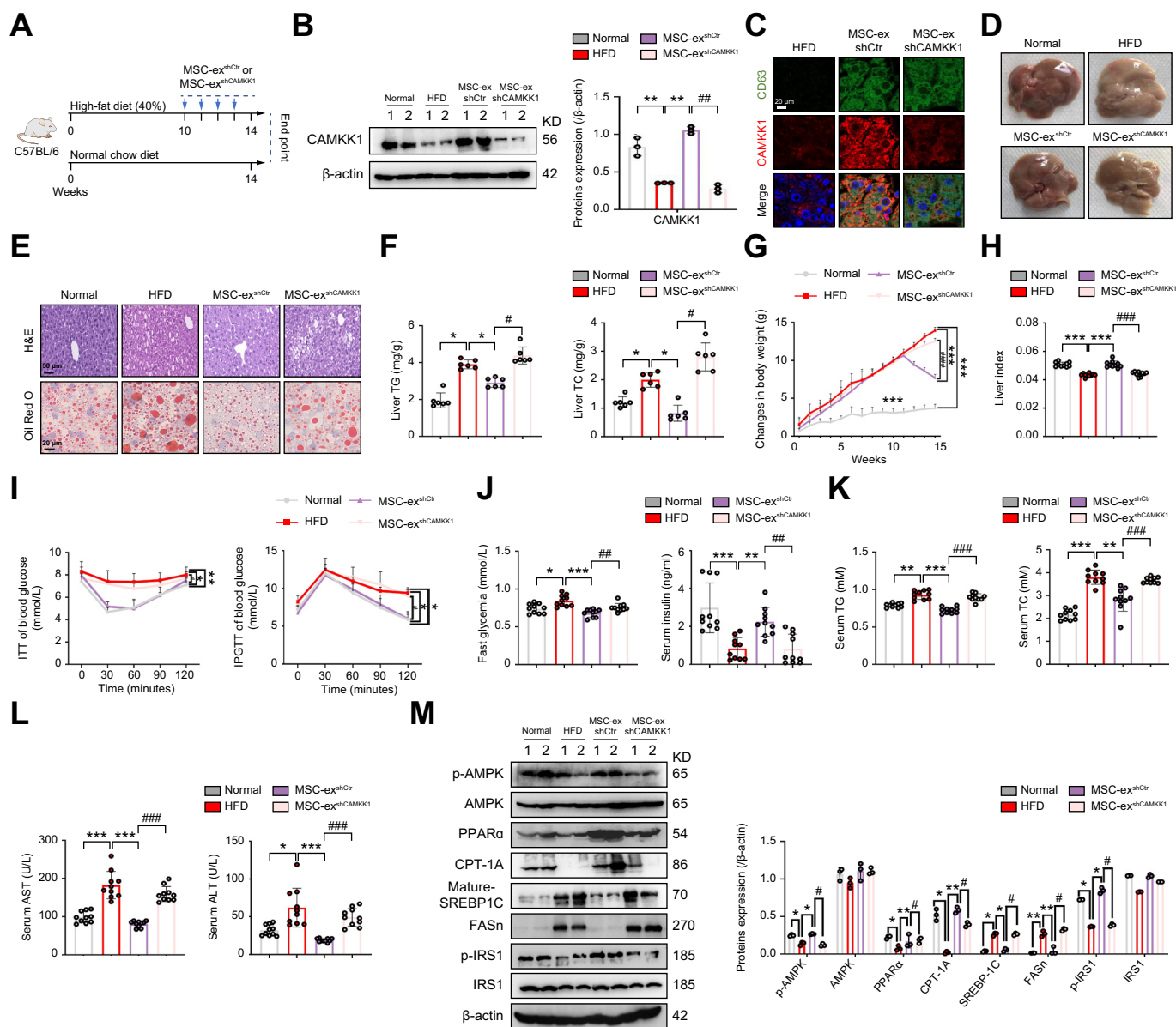
Fig. 7. Knockdown of CAMKK1 in MSC-ex increases hepatic lipid accumulation and injury in HFD-fed mice. (A) C57BL/6 mice were placed on a HFD (40%) and administered 10 mg/kg of MSC-ex^{shCtr} or MSC-ex^{shCAMKK1} i.v. from the 10th week to the 14th week of HFD feeding. As a control, the same volume of PBS was injected. (B) Immunoblotting analyses of CAMKK1 proteins in mice and quantification of the results. (C) Representative immunofluorescence confocal microscopy images of CD63 (green) and CAMKK1 (red) colocalisation; nuclei were labelled with DAPI (blue). Scale bars, 20 μm. (D) Representative images of gross liver appearance for mice fed a normal chow diet (normal group) or HFD for 10 weeks and then injected with PBS, MSC-ex^{shCtr}, or MSC-ex^{shCAMKK1} for 4 weeks. (E) Representative images of H&E (top; scale bars, 50 μm) and Oil Red O (bottom; Scale bars, 20 μm) staining of liver sections. (F) Liver contents of total TG and TC, n = 10 per group. (G) Body weight changes of mice. (H) Changes in the liver indexes of mice (liver index = liver wet weight/body weight). (I) i.p. ITTs evaluated individual insulin tolerance by injecting insulin at a dose of 0.75 IU/kg body weight; blood glucose levels were detected at 0, 30, 60, 90, and 120 min and compared with that at 0 min. Individual glucose tolerance was assessed by IPGTT; fasted mice were administered 1 g of glucose/kg body weight by i.p. injection, and blood glucose levels were determined at 0, 30, 60, 90, and 120 min. (J) Fasting glycaemia (after 16-h fast) and serum insulin levels, n = 10 per group. (K and L) Serum TG and TC (K), and AST and ALT (L) levels, n = 10 per group. (M) Immunoblotting analyses of AMPK signalling proteins in livers and quantification. Data are represented as the mean ± SEM. Statistical analyses by a one-way ANOVA (F–M). $^*p <0.05$, $^{**}p <0.01$, $^{***}p <0.001$ *vs.* HFD group; $^#p <0.05$, $^{##}p <0.01$, $^{###}p <0.001$ *vs.* MSC-ex^{shCtr} (10 mg/kg) group. ALT, alanine transaminase; AMPK, AMP-activated protein kinase; AST, aspartate transaminase; CAMKK1, calcium/calmodulin-dependent protein kinase 1; CPT-1A, carnitine palmitoyltransferase 1A; FASn, fatty acid synthase; HFD, high-fat diet; IPGTT, i.p. glucose tolerance test; IRS1, insulin receptor substrate 1; ITT, insulin tolerance test; MSC-ex, MSC-derived exosomes; MSC, mesenchymal stem cell; p-AMPK, phosphorylated AMPK; p-IRS1, phosphorylated IRS1; PPARα, peroxisome proliferator-activated receptor alpha; SREBP-1C, sterol regulatory element-binding protein-1C; TC, total cholesterol; TG, triglycerides.

increased in MSC-ex^shCtr mice but not in MSC-ex^shCAMKK1 mice (Fig. 7B). Immunofluorescence revealed colocalisation of CAMKK1 with the exosomal marker CD63 in livers in MSC-ex^shCtr- and MSC-ex^shCAMKK1-injected HFD mice (Fig. 7C). Macroscopic examination showed that MSC-ex^shCtr appeared normal on the gross liver appearance but that the livers of the MSC-ex^shCAMKK1 administration group remained pale yellow (Fig. 7D). H&E and Oil Red O staining revealed that MSC-ex^shCtr, but not MSC-ex^shCAMKK1, was able to reduce hepatocyte vacuolation and lipid accumulation (Fig. 7E). Consistently, MSC-ex-mediated reduction in liver TG, TC, and body weight and promotion in the liver index were abolished by CAMKK1 knockdown (Fig. 7F–H). Less weight gain of inguinal adipose tissue was found in MSC-ex^shCtr than in MSC-ex^shCAMKK1 mice (Fig. S6A). The food intake was not significantly altered between the groups of mice throughout the treatment period (Fig. S6B). In addition, results of ITT and IPGTT showed that the ability of MSC-ex^shCtr to control blood glucose in HFD mice was diminished by MSC-ex^shCAMKK1 (Fig. 7I). MSC-ex^shCtr reduced fasting blood glucose and increased serum insulin, and these were reversed by MSC-ex^shCAMKK1 (Fig. 7J). The levels of serum TG, TC, AST, and ALT were also decreased in the MSC-ex^shCtr group but not in the MSC-ex^shCAMKK1 group (Fig. 7K and L). Furthermore, the regulatory effect of MSC-ex^shCtr on p-AMPK/PPARα/CPT-1A signalling and reduced SREBP-1c/FASn signalling in livers from HFD mice was abolished by CAMKK1 knockdown in MSC-ex^shCAMKK1 mice (Fig. 7M). Similarly, the expression of inflammatory factors in the livers of mice fed a HFD was also reduced by MSC-ex^shCtr but not by MSC-ex^shCAMKK1 (Fig. S6C). Collectively, these results provide *in vivo* evidence that CAMKK1 is required for MSC-ex-dependent regulation of lipid metabolism in NAFLD, thus verifying that CAMKK1 is an essential factor for MSC-ex-mediated anti-hepatic steatosis and liver protection.

Discussion

NAFLD includes many conditions, from simple steatosis to non-alcoholic steatohepatitis, which can lead to fibrosis, cirrhosis, and even hepatocellular carcinoma.[29] It is also associated with metabolic syndromes such as diabetes mellitus, obesity, and hypertension.[30] Because liver steatosis plays an important role in the pathogenesis of NAFLD, agents that significantly affect liver steatosis may serve as potential therapeutic candidates for NAFLD.[31] So far, there is no approved drug for treating liver steatosis.[3,32] Exosomes contain bioactive factors, such as proteins, lipids, mRNAs, microRNAs, and lncRNAs,[33] and thus are candidate therapeutics for various diseases via their potential to shift cellular signalling repertoires. Furthermore, MSCs have been shown to increase the expression of fatty acid oxidation-related genes in obese type 2 diabetic mice,[34] promote the oxidation of fatty acids in hepatocytes post hepatectomy liver failure,[35] and upregulate fatty acid oxidation in breast cancer[36] or gastric cancer cells.[37] Increasing evidence shows that MSC-ex inhibit hepatocyte apoptosis, promote hepatocyte proliferation, and reduce inflammation responses.[38] Furthermore, Cheng *et al.*[14] recently reported that human umbilical cord MSC-ex reduce the expression of lipid metabolism-related proteins (FAS, SREBP-1C, and PPARα) and inhibit lipid deposition in

NAFLD rats. However, the role of MSC-ex in liver steatosis is not fully understood, and the mechanisms have not been elucidated.

In the present study, we report that human umbilical cord MSC-ex suppress lipid deposition and improves liver function in HFD-induced liver steatosis mice. In OPA-treated human hepatocyte L02 cells, the fatty acid oxidation rate was increased, and lipid metabolites were reduced by MSC-ex treatment. Moreover, exosomal CAMKK1 contributed to MSC-ex-mediated liver steatosis alleviation in an AMPK-dependent manner. In OPA-treated L02 cells, the fatty acid oxidation rate was approximately 1.75-fold increased, and 31 of 34 (91.18%) of the lipid metabolites were reduced by MSC-ex. Therefore, our study verifies the anti-hepatic steatosis role of MSC-ex and expands our understanding of its therapeutic potential.

Our results reveal several signalling mediators that underlie the protective effects of MSC-ex, including AMPK, which was demonstrated to act as a central regulator in MSC-ex-mediated fatty acid oxidation and fatty acid synthesis suppression. MSC-ex treatment activated AMPK-mediated PPARα/CPT-1A and the SREBP-1C/FASn signalling pathway, consistent with previous data.[39] To clarify how MSC-ex regulate the AMPK signalling pathway, we analysed the protein profile in MSC-ex by LC-MS/MS. Our data indicate that abundant CAMKK1 in MSC-ex is transported to liver tissues and hepatocytes. Furthermore, we demonstrated that CAMKK1 plays an essential role in MSC-ex-mediated AMPK activation and anti-hepatic steatosis in L02 cells. These results are consistent with evidence that AMPK is the primary downstream target of CAMKK2.[40] We also demonstrated that CAMKK1 knockdown in MSC-ex reduces anti-hepatic steatosis activity *in vitro* and *in vivo*, suggesting that exosomal CAMKK1 may be critical for MSC-ex-mediated anti-hepatic steatosis and liver protection. Thus, these results prove that CAMKK1 can activate AMPK and regulate lipid metabolism in liver disease.

Although this study shows important discoveries, there are also limitations. First, we used a single effective dose of MSC-ex; however, animal experiments need to further define the optimal dose described. Second, the specific mechanism by which MSC-ex regulate lipid metabolism has yet to be determined. Evidence indicates that reduced fatty acid oxidation and increased lipid synthesis in the liver lead to the accumulation of liver lipids, ultimately leading to hepatic steatosis.[31] Therefore, studying fatty acid oxidation and lipid synthesis will be particularly important. Third, MSC-ex have been demonstrated to contain a variety of bioactive molecules and exert effects on diverse liver cell types to improve liver injury.[41] Many pathogenic factors also play an essential role in developing hepatic steatosis.[42] Thus, MSC-ex likely exert a therapeutic role by transferring additional factors to additional cell types that contribute to its therapeutic effect on steatosis. Whether MSC-ex can inhibit steatosis by regulating insulin resistance and mitochondrial abnormalities is also not clear. Therefore, further detailed investigation of exosomal factors and contributing mechanisms of action of MSC-ex is necessary.

In conclusion, we demonstrated that MSC-ex effectively reduce lipid deposition in hepatocytes and improve liver function from HFD-induced liver steatosis. MSC-ex confer anti-hepatic steatosis effects against lipid deposition *in vitro* and

in vivo. These effects may be mediated by the delivery of CAMKK1 to promote fatty acid oxidation and suppress fatty acid synthesis via AMPK-mediated PPARα/CPT-1A and SREBP-1C/FASn signalling. Therefore, our findings are significant in elucidating novel mechanisms related to MSC-ex-based therapies for preventing hepatic steatosis.

Abbreviations

AFM, atomic force microscopy; ALT, alanine transaminase; AML12, alpha mouse liver 12; AMPK, AMP-activated protein kinase; AST, aspartate transaminase; CAMKK1, calcium/calmodulin-dependent protein kinase 1; CCK-8, Cell Counting Kit-8; CPT-1A, carnitine palmitoyltransferase 1A; deMSC-ex, MSC-ex-free conditional medium supernatant; FASn, fatty acid synthase; FDA, fluorescein diacetate; GFP, green fluorescent protein; HFD, high-fat diet; HFL1-ex, foetal HFL1-derived exosomes; HFL1, human lung fibroblast 1; IGFL2, insulin growth factor-like family member 2; IPGTT, i.p. glucose tolerance test; IRS1, insulin receptor substrate 1; ITT, insulin tolerance test; KEGG, Kyoto Encyclopedia of Genes and Genomes; LC-MS, liquid chromatography; MS, mass spectrometry; MS/MS, tandem MS; MSC-ex, MSC-derived exosomes; MSC, mesenchymal stem cell; NAFLD, non-alcoholic fatty liver disease; OPA, oleic–palmitic acid; p-AMPK, phosphorylated AMPK; p-IRS1, phosphorylated IRS1; PPARα, peroxisome proliferator-activated receptor alpha; PRKAG1, protein kinase AMP-activated non-catalytic subunit gamma 1; QRT-PCR, quantitative reverse transcription-PCR; SREBP-1C, sterol regulatory element-binding protein-1C; TC, total cholesterol; TEM, transmission electron microscopy; TG, triglycerides; TNF, tumour necrosis factor; TSG101, tumour susceptibility gene 101.

Conflicts of interest

The authors declare no competing financial interest.

Please refer to the accompanying ICMJE disclosure forms for further details.

Authors' contributions

Conceptualisation, data curation, formal analysis, and writing the original draft: FY, JJ. Investigation and methodology: FY, YW, YC, JX, YC. Funding acquisition, project administration, and supervision: YY.

Data availability statement

Gene expression RNA-seq data have been deposited in the NCBI, and the SRA accession number is SRP337303. Non-targeted lipidomics data have been deposited in the MetaboLights, with MTBLS3452 (www.ebi.ac.uk/metabolights/MTBLS3452) as the accession number. The authors declare that all data supporting the findings of this study are available in figshare (https://figshare.com/s/bc29a1aec8e64d5d7ecb). Other data are available from the corresponding author upon request.

Supplementary data

Supplementary data to this article can be found online at https://doi.org/10.1016/j.jhepr.2023.100746.

References

Author names in bold designate shared co-first authorship

[1] Adams LA, Waters OR, Knuiman MW, Elliott RR, Olynyk JK. NAFLD as a risk factor for the development of diabetes and the metabolic syndrome: an eleven-year follow-up study. Am J Gastroenterol 2009;104:861–867.

[2] Younossi Z, Anstee QM, Marietti M, Hardy T, Henry L, Eslam M, et al. Global burden of NAFLD and NASH: trends, predictions, risk factors and prevention. Nat Rev Gastroenterol Hepatol 2018;15:11–20.

[3] Radaelli MG, Martucci F, Perra S, Accornero S, Castoldi G, Lattuada G, et al. NAFLD/NASH in patients with type 2 diabetes and related treatment options. J Endocrinol Invest 2018;41:509–521.

[4] Lee CW, Hsiao WT, Lee OK. Mesenchymal stromal cell-based therapies reduce obesity and metabolic syndromes induced by a high-fat diet. Transl Res 2017;182:61–74 e68.

[5] Cao M, Pan Q, Dong H, Yuan X, Li Y, Sun Z, et al. Adipose-derived mesenchymal stem cells improve glucose homeostasis in high-fat diet-induced obese mice. Stem Cel Res Ther 2015;6:208.

[6] **Zhao S**, **Liu Y**, Pu Z. Bone marrow mesenchymal stem cell-derived exosomes attenuate D-GalN/LPS-induced hepatocyte apoptosis by activating autophagy in vitro. Drug Des Devel Ther 2019;13:2887–2897.

[7] Walldorf J, Hillebrand C, Aurich H, Stock P, Hempel M, Ebensing S, et al. Propranolol impairs liver regeneration after partial hepatectomy in C57Bl/6-mice by transient attenuation of hepatic lipid accumulation and increased apoptosis. Scand J Gastroenterol 2010;45:468–476.

[8] **Qian H**, **Ding X**, **Zhang J**, Mao F, Sun Z, Jia H, et al. Cancer stemness and metastatic potential of the novel tumor cell line K3: an inner mutated cell of bone marrow-derived mesenchymal stem cells. Oncotarget 2017;8:39522–39533.

[9] Toh WS, Lai RC, Hui JHP, Lim SK. MSC exosome as a cell-free MSC therapy for cartilage regeneration: implications for osteoarthritis treatment. Semin Cel Dev Biol 2017;67:56–64.

[10] Tetta C, Ghigo E, Silengo L, Deregibus MC, Camussi G. Extracellular vesicles as an emerging mechanism of cell-to-cell communication. Endocrine 2013;44:11–19.

[11] Yan Y, Jiang W, Tan Y, Zou S, Zhang H, Mao F, et al. hucMSC exosome-derived GPX1 is required for the recovery of hepatic oxidant injury. Mol Ther 2017;25:465–479.

[12] **Li T**, **Yan Y**, Wang B, Qian H, Zhang X, Shen L, et al. Exosomes derived from human umbilical cord mesenchymal stem cells alleviate liver fibrosis. Stem Cell Dev 2013;22:845–854.

[13] **Ding H-R**, **Wang J-L**, Tang Z-T, Wang Y, Zhou G, Liu Y, et al. Mesenchymal stem cells improve glycometabolism and liver regeneration in the treatment of post-hepatectomy liver failure. Front Physiol 2019;10:412.

[14] Cheng L, Yu P, Li F, Jiang X, Jiao X, Shen Y, et al. Human umbilical cord-derived mesenchymal stem cell-exosomal miR-627-5p ameliorates non-alcoholic fatty liver disease by repressing FTO expression. Hum Cel 2021;34:1697–1708.

[15] Watanabe T, Tsuchiya A, Takeuchi S, Nojiri S, Yoshida T, Ogawa M, et al. Development of a non-alcoholic steatohepatitis model with rapid accumulation of fibrosis, and its treatment using mesenchymal stem cells and their small extracellular vesicles. Regen Ther 2020;14:252–261.

[16] **Sun Y**, **Shi H**, **Yin S**, Ji C, Zhang X, Zhang B, et al. Human mesenchymal stem cell derived exosomes alleviate type 2 diabetes mellitus by reversing peripheral insulin resistance and relieving beta-cell destruction. ACS Nano 2018;12:7613–7628.

[17] Qiao C, Xu W, Zhu W, Hu J, Qian H, Yin Q, et al. Human mesenchymal stem cells isolated from the umbilical cord. Cell Biol Int 2008;32:8–15.

[18] Gómez-Lechón MJ, Donato MT, Martínez-Romero A, Jiménez N, Castell JV, O'Connor J-E. A human hepatocellular in vitro model to investigate steatosis. Chem Biol Interact 2007;165:106–116.

[19] **Fang S-B**, **Zhang H-Y**, **Wang C**, He BX, Liu XQ, Meng XC, et al. Small extracellular vesicles derived from human mesenchymal stromal cells prevent group 2 innate lymphoid cell-dominant allergic airway inflammation through delivery of miR-146a-5p. J Extracell Vesicles 2020;9:1723260.

[20] Woo CH, Kim HK, Jung GY, Jung YJ, Lee KS, Yun YE, et al. Small extracellular vesicles from human adipose-derived stem cells attenuate cartilage degeneration. J Extracell Vesicles 2020;9:1735249.

[21] **Asgharpour A**, **Cazanave SC**, Pacana T, Seneshaw M, Vincent R, Banini BA, et al. A diet-induced animal model of non-alcoholic fatty liver disease and hepatocellular cancer. J Hepatol 2016;65:579–588.

[22] Greenspan P, Mayer EP, Fowler SD. Nile red: a selective fluorescent stain for intracellular lipid droplets. J Cel Biol 1985;100:965–973.

[23] Xu Y, Huang J, Xin W, Chen L, Zhao X, Lv Z, et al. Lipid accumulation is ahead of epithelial-to-mesenchymal transition and therapeutic intervention by acetyl-CoA carboxylase 2 silence in diabetic nephropathy. Metabolism 2014;63:716–726.

[24] Gandham S, Su X, Wood J, Nocera AL, Alli SC, Milane L, et al. Technologies and standardization in research on extracellular vesicles. Trends Biotechnol 2020;38:1066–1098.

[25] Ruderman NB, Carling D, Prentki M, Cacicedo JM. AMPK, insulin resistance, and the metabolic syndrome. J Clin Invest 2013;123:2764–2772.

[26] Montagner A, Polizzi A, Fouché E, Ducheix S, Lippi Y, Lasserre F, et al. Liver PPARα is crucial for whole-body fatty acid homeostasis and is protective against NAFLD. Gut 2016;65:1202–1214.

[27] Zhang B, Wu X, Zhang X, Sun Y, Yan Y, Shi H, et al. Human umbilical cord mesenchymal stem cell exosomes enhance angiogenesis through the Wnt4/β-catenin pathway. Stem Cell Transl Med 2015;4:513–522.

[28] Hawley SA, Pan DA, Mustard KJ, Ross L, Bain J, Edelman AM, et al. Calmodulin-dependent protein kinase kinase-beta is an alternative upstream kinase for AMP-activated protein kinase. Cell Metab 2005;2:9–19.

[29] Cotter TG, Rinella M. Nonalcoholic fatty liver disease 2020: the state of the disease. Gastroenterology 2020;158:1851–1864.

[30] Tilg H, Moschen AR, Roden M. NAFLD and diabetes mellitus. Nat Rev Gastroenterol Hepatol 2017;14:32–42.

[31] Kong Q, Zhang H, Zhao T, Zhang W, Yan M, Dong X, et al. Tangshen formula attenuates hepatic steatosis by inhibiting hepatic lipogenesis and augmenting fatty acid oxidation in db/db mice. Int J Mol Med 2016;38:1715–1726.

[32] Cardoso AC, de Figueiredo-Mendes C, Villela-Nogueria CA, Sanyal AJ. New drugs for non-alcoholic steatohepatitis. Liver Int 2020;40(Suppl. 1):96–101.

[33] Akers JC, Gonda D, Kim R, Carter BS, Chen CC. Biogenesis of extracellular vesicles (EV): exosomes, microvesicles, retrovirus-like vesicles, and apoptotic bodies. J Neurooncol 2013;113:1–11.

[34] Li B, Cheng Y, Yu S, Zang L, Yin J, Liu J, et al. Human umbilical cord-derived mesenchymal stem cell therapy ameliorates nonalcoholic fatty liver disease in obese type 2 diabetic mice. Stem Cell Int 2019;2019:8628027.

[35] Wang J-L, Ding H-R, Pan C-Y, Shi X-L, Ren H-Z. Mesenchymal stem cells ameliorate lipid metabolism through reducing mitochondrial damage of hepatocytes in the treatment of post-hepatectomy liver failure. Cell Death Dis 2021;12:111.

[36] Han J, Qu H, Han M, Ding Y, Xie M, Hu J, et al. MSC-induced lncRNA AGAP2-AS1 promotes stemness and trastuzumab resistance through regulating CPT1 expression and fatty acid oxidation in breast cancer. Oncogene 2021;40:833–847.

[37] He W, Liang B, Wang C, Li S, Zhao Y, Huang Q, et al. MSC-regulated lncRNA MACC1-AS1 promotes stemness and chemoresistance through fatty acid oxidation in gastric cancer. Oncogene 2019;38:4637–4654.

[38] Eguchi A, Feldstein AE. Extracellular vesicles in non-alcoholic and alcoholic fatty liver diseases. Liver Res 2018;2:30–34.

[39] Tian X, Ru Q, Xiong Q, Wen R, Chen Y. Catalpol attenuates hepatic steatosis by regulating lipid metabolism via AMP-activated protein kinase activation. Biomed Res Int 2020;2020:6708061.

[40] Woods A, Dickerson K, Heath R, Hong SP, Momcilovic M, Johnstone SR, et al. Ca^{2+}/calmodulin-dependent protein kinase kinase-β acts upstream of AMP-activated protein kinase in mammalian cells. Cel Metab 2005;2:21–33.

[41] Dorairaj V, Sulaiman SA, Abu N, Abdul Murad NA. Extracellular vesicles in the development of the non-alcoholic fatty liver disease: an update. Biomolecules 2020;10:1494.

[42] Koliaki C, Roden M. Alterations of mitochondrial function and insulin sensitivity in human obesity and diabetes mellitus. Annu Rev Nutr 2016;36:337–367.